JPL PUBLICATION 82-45

Spacecraft Drag-Free Technology Development

On-Board Estimation and Control Synthesis

R.W. Key
E. Mettler
M.H. Milman
D.B. Schaechter

May 15, 1982

National Aeronautics and
Space Administration

Jet Propulsion Laboratory
California Institute of Technology
Pasadena, California

JPL PUBLICATION 82-45

Spacecraft Drag-Free Technology Development

On-Board Estimation and Control Synthesis

R.W. Key
E. Mettler
M.H. Milman
D.B. Schaechter

May 15, 1982

NASA
National Aeronautics and
Space Administration

Jet Propulsion Laboratory
California Institute of Technology
Pasadena, California

The research described in this publication was carried out by the Jet Propulsion Laboratory, California Institute of Technology, under contract with the National Aeronautics and Space Administration.

ABSTRACT

This report presents research into estimation and control methods for a "Drag-Free" spacecraft. This work represents the functional and analytical synthesis of on-board estimators and controllers for an integrated attitude and translation control system. An earlier study [4] addressed the general feasibility of a drag-free STARPROBE (Solar Probe) spacecraft. This effort pursues the basic issues raised in the preceding study and creates the framework for detail definition and design of the baseline drag-free system. The techniques for solution of self-gravity and electrostatic charging problems are applicable generally, as is the control system development.

Table of Contents

SPACECRAFT DRAG-FREE TECHNOLOGY DEVELOPMENT

On-Board Estimation and Control Synthesis

List of Tables

List of Figures

I. INTRODUCTION

A. Background

The Starprobe spacecraft has been designed for a study of the nearest star to Earth, the Sun. Three classes of experiments have been identified for the Starprobe mission. These are: fields and particles experiments, imaging science experiments, and radiometric/gravitational experiments. The perihelion distance of four solar radii will provide a unique opportunity for obtaining this science data.

The close passage of Starprobe to the Sun also allows for precision gravitational experiments to be performed. Using Earth-based tracking and a model of the sun's gravitational field, it will be possible to extract parameters which describe the sun's gravitational potential. There is specific interest in extracting the sun's quadrupole moment, J_2, and possibly higher harmonics, as well as gravitational parameters which arise due to relativistic effects of the sun. However, non-gravitational effects, such as solar pressure, would result in such large uncertainties in the gravitational model that little useful information would be obtained. Fortunately, these non-gravitational effects can be almost entirely removed by incorporation of a "drag-free" translation control system. The drag-free control system concept has been demonstrated on TRIAD, an Earth orbiting satellite, and non-gravitational spacecraft accelerations were shown to be reduced to a level of 5×10^{-12} g's. The Starprobe spacecraft with such a control system in conjunction with ground tracking would be able to provide valuable information on the sun's gravitational field.

B. New Issues

The drag-free system on TRIAD operated at the level of 5×10^{-12} g's. This would certainly be adequate for Starprobe. However, significant

differences exist between these two spacecraft and their mission environments. The gravity-gradient stabilized TRIAD spacecraft was dedicated to proof of the drag-free control concept. As such, the entire spacecraft was configured around this drag-free instrumentation. Moving, or variable masses were kept to a minimum, and were physically located on booms a large distance from the drag-free sensor. The electromagnetic environment was benign for the 800 km Earth orbiting TRIAD. On the other hand the multi-experiment Starprobe is not uniquely configured around the drag-free system. In fact it is necessary to achieve the required drag-free performance in spite of relaxation in spacecraft configuration constraints. Specifically, Starprobe will differ from TRIAD in the following aspects.

1) The Starprobe drag-free control system will not necessarily be located at the spacecraft center of mass. This will produce coupling between the attitude control and translation control systems. This effect is especially pronounced during imaging slews of the spacecraft (both cross-track and in-track during which time drag-free accuracy must be maintained).

2) The Starprobe drag-free control system must operate in spite of moving antenna, articulated instruments, fuel depletion, and spacecraft thermal distortions. These effects may all result in self-gravity disturbances.

3) The Starprobe drag-free control system may operate in severe electromagnetic and high energy particle environments (solar and Jovian)[7]. Should the proof mass attain a net charge due to this environment, electrostatic forces will degrade the drag-free trajectory. (See also Appendix E.)

C. Purpose of the On-Board Estimator

To some extent, increased computational work on board the spacecraft can compensate for some of the previously mentioned "new issues." This additional computation takes the form of an on-board estimator.

The basic purpose of the on-board estimator is to provide state information for the attitude/translation control system; to incorporate sensed mass redistribution and the proof mass position for an integrated proof mass trajectory determination; and to either identify, or minimize the effects of proof mass charge.

The focus of this report will be on the various aspects of drag-free estimation and control for Starprobe. The relevant dynamics will be presented, first. This will be followed by sections devoted to each of the new issue areas for drag-free control. The results will then be discussed and future research needs identified.

II. DYNAMICS

In order to describe the proof mass trajectory around the sun, and the rotational and translational dynamics of the spacecraft, four vector equations of motion are required. Prior to presenting these equations, several figures will be presented here for concreteness, and for future reference.

The first figure (Fig. 1) illustrates the nominal trajectory of the spacecraft around the sun. The trajectory takes the spacecraft from north of the ecliptic plane to south of the ecliptic plane. The magnified view of the trajectory shows the spacecraft nadir pointed.

Figure 2 shows the spacecraft fixed coordinate system. The +z axis is in the shield direction, the +x axis is up, and the +y axis is out of the page. This coordinate system will be adhered to for all translational and rotational motions and analysis.

Finally, Fig. 3 is a schematic of the proof mass in the proof mass cavity. Note that the center of mass of the spacecraft does not coincide with the center of the cavity in this illustration.

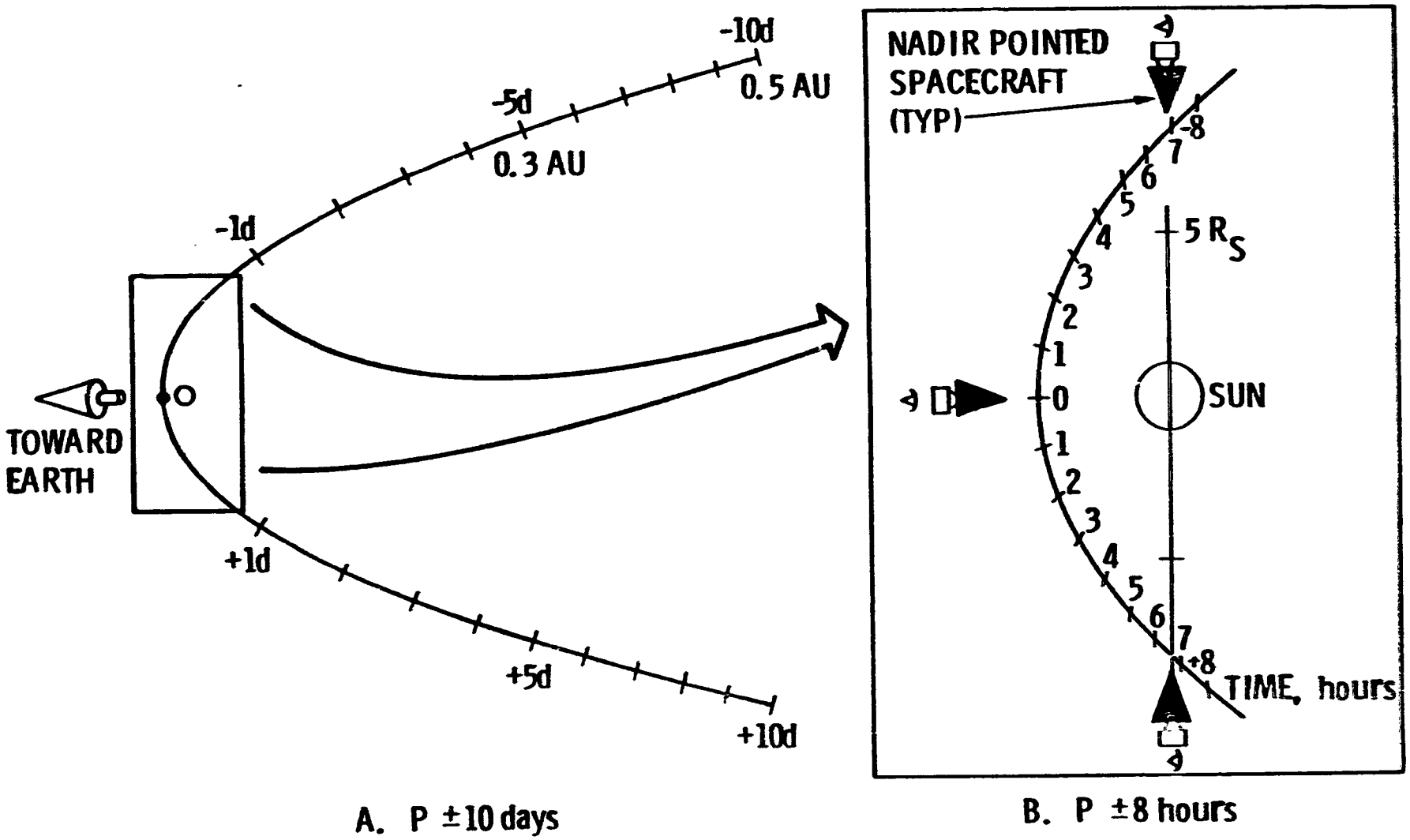

Figure 1. Near-Perihelion Trajectory (Perihelion Radius = $4R_S$, Inclination = 90 Degrees)

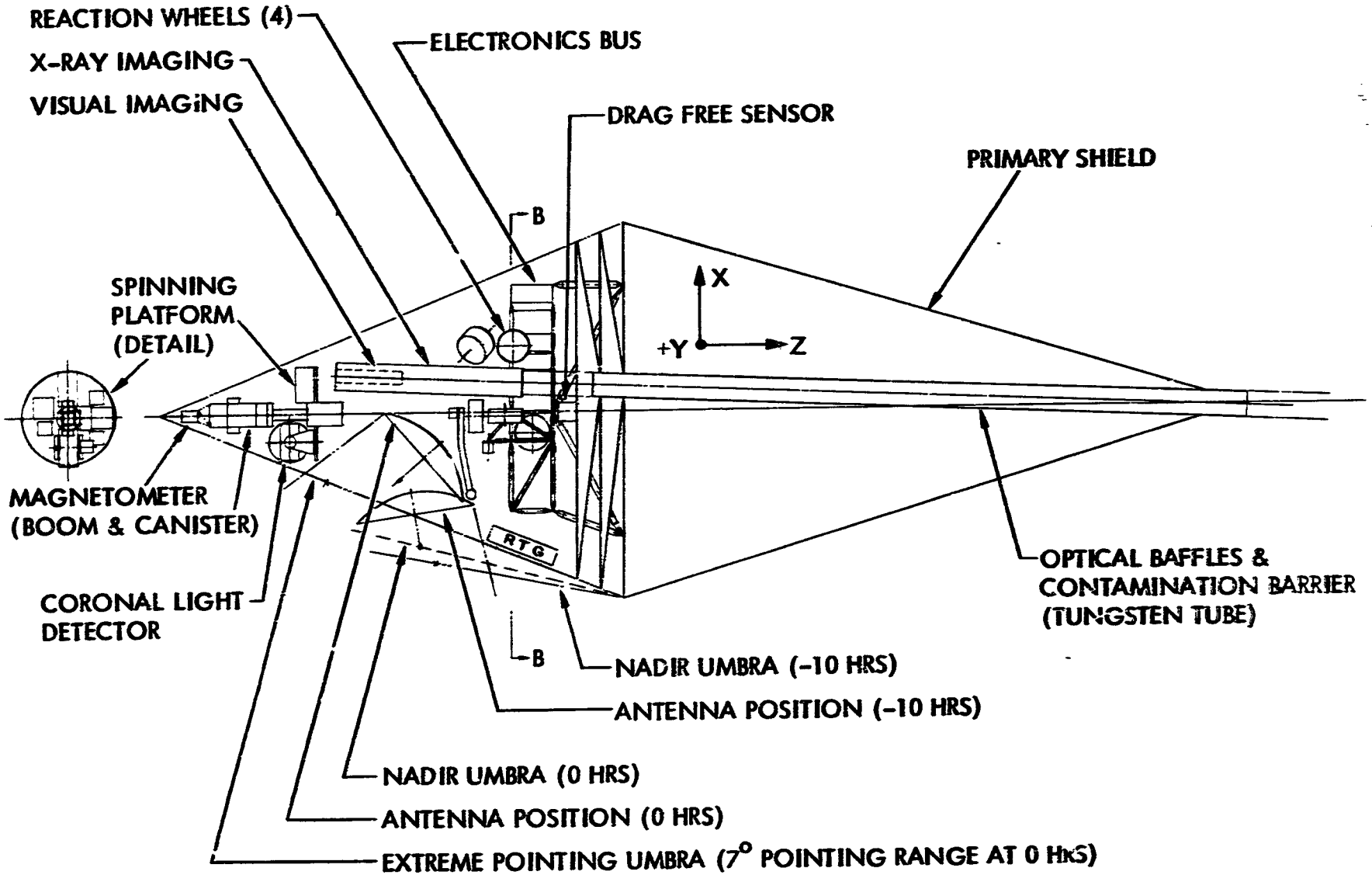

Figure 2. Full Science Configuration
(Side View at Perihelion)

Figure 3. Proof Mass and Cavity Schematic
(Not to Scale)

A. Orbital Dynamics

It is the shielded proof mass itself that follows a ballistic drag-free trajectory around the sun. The remainder of the spacecraft performs continuous stationkeeping about the proof mass, so the entire spacecraft is drag-free. Let R be the vector from the sun to the proof mass, then the orbital equations of motion for the proof mass is given by

$$m\ddot{\vec{R}} = \nabla U(\vec{R}) + \vec{F}_{el} + \vec{F}_{sg} \qquad (2.1)$$

In (2.1) U is the scalar gravitational potential of the Sun; F_{el} and F_{sg} are electrostatic and self-gravity forces respectively; m is the mass of the proof mass. It can be seen in the absence of electroctatic and self-gravity forces, and to the accuracy retained here, the proof mass follows a purely gravitational path. It is therefore vital to minimize directly the electrostatic and self-gravity forces, and to know indirectly their residual effects on the trajectory of the spacecraft.

B. Spacecraft Translational Dynamics

For the spacecraft as a whole to fly drag-free, a control system must be implemented to maintain the spacecraft relative to the proof mass. A prerequisite to controlling the spacecraft in such a manner is a model of the spacecraft dynamics with respect to the proof mass. Letting M be the mass of the spacecraft, $\vec{\rho}$, the vector from the center of the cavity to the spacecraft mass center, and $\vec{r}$ the vector from the center of the cavity to the proof mass, the equations of motion of the spacecraft center of mass may be written with respect to the (inertial) proof mass as follows

$$M(\ddot{\vec{\rho}} - \ddot{\vec{r}}) = \vec{F}_c + \vec{F}_{sp} \qquad (2.2)$$

Again, to the accuracy retained in this model, the only forces shown affecting the spacecraft are the control forces, $\vec{F}_c$, and the solar pressure force, $\vec{F}_{sp}$. The objective of the translation control system is to keep $\vec{r}$ small, i.e., keep the spacecraft centered around the proof mass in spite of some center of mass offset. The solar pressure force is continuous in nature, while the control force is produced by on-off translation thrusters.

C. Spacecraft Rotational Dynamics

Certainly, attitude control is a vital part of the Starprobe mission. However, in the past attitude control has usually not been a part of a drag-free translation control system. The reason that the topic of attitude control must be discussed for the Starprobe drag-free control system is due to center of mass offset from the center of the cavity. Looking at Fig. 3, it can be seen that even if the proof mass is at the center of the cavity, a rotation of the spacecraft about its mass center will produce a relative motion of the proof mass in the cavity. Essentially, if the center of mass of the spacecraft is offset from the cavity center, control fuel will have to be expended in order to cause the spacecraft to rotate about the center of the cavity, rather than about its center of mass. The rotational dynamics of the spacecraft may be simply written as

$$\frac{d}{dt}\left(\vec{\vec{I}} \cdot \vec{\omega}\right) = \vec{T}_c + \vec{T}_{sp} \qquad (2.3)$$

$\vec{\vec{I}}$ is the spacecraft inertia tensor, $\vec{\omega}$ is the spacecraft angular velocity, and T_c and T_{sp} are control torques and solar pressure torques respectively.

D. Charge Interaction

The Starprobe drag-free control system must operate in a harsh electromagnetic and high energy particle environment, [7]. Since the proof

mass must remain isolated from the remainder of the spacecraft to achieve drag-free performance, the possibility of the proof mass acquiring a net charge arises. Of course, if the proof mass does become charged, electrostatic forces will cause it to be attracted to the spacecraft and thus deteriorate the drag-free performance. In order to reduce the impact of proof mass charge, a good understanding of how the charge affects the proof mass dynamics must be available. The model used for these studies is given as

$$m \ddot{\vec{r}} = \vec{F}_{el} \tag{2.4}$$

where all the terms have been previously defined. It should be noted that the exact form of the electrostatic force as a function of the proof mass charge, the proof mass position, and the voltages on the capacitive proof mass position sensor plates has been an area of parallel research.[1,2]

III. SPACECRAFT ATTITUDE AND TRANSLATION CONTROL SYSTEM

A. Control Objectives

The STARPROBE control system is a complete 6-degree-of-freedom design which provides both attitude and translation control on all three spacecraft axes. Spacecraft attitude control will be required throughout the entire mission while translation control is required mainly for the drag-free solar encounter phase of the mission. The functional objectives of the total control system can be summarized as follows:

1) Maintain highly accurate and stable pointing control of the spacecraft relative to the sun and an inertial attitude reference frame.

2) Provide precise drag compensation and translation control of the spacecraft relative to the proof-mass trajectory reference.

3) Minimize the control gas usage and the translation thrusters on/off cycles, especially during the solar encounter when there is a one-sided solar pressure force acting on the spacecraft.

4) Minimize the disturbances on the proof mass trajectory due to spacecraft-proof mass dynamic interactions which arise from sources such as electrostatic charges and self-gravity.

Performance requirements for this control system are derived from science experiment objectives, spacecraft design considerations, and the environments through which the spacecraft is expected to pass. Science objectives were discussed earlier in this report and spacecraft design considerations have been studied in other reports.[5,6] The problems of integrating a combined attitude/translation control system into a spacecraft with constraints on mass, power consumption, and unique thermal shielding pose significant limitations on the control system design. For example, the thermal shielding will necessitate that some of the control system gas jets be canted with respect to the major axes of the spacecraft, thus causing a decrease in the usable amount of control force and an increase in the amount of fuel needed to sufficiently maintain control. For reasons such as this, it is very important to optimize the way in which control actions are taken so as to maximize their effect and minimize the fuel required. The control system design concept that is currently being developed to provide this kind of optimized control is shown schematically in Figure 4. The figure shows not only the spacecraft dynamics but also the proof mass dynamics. Because the two are coupled, the overall system performance is dependent on both. A complete description of this figure and a computer simulation program that is based on it is presented in the following subsections.

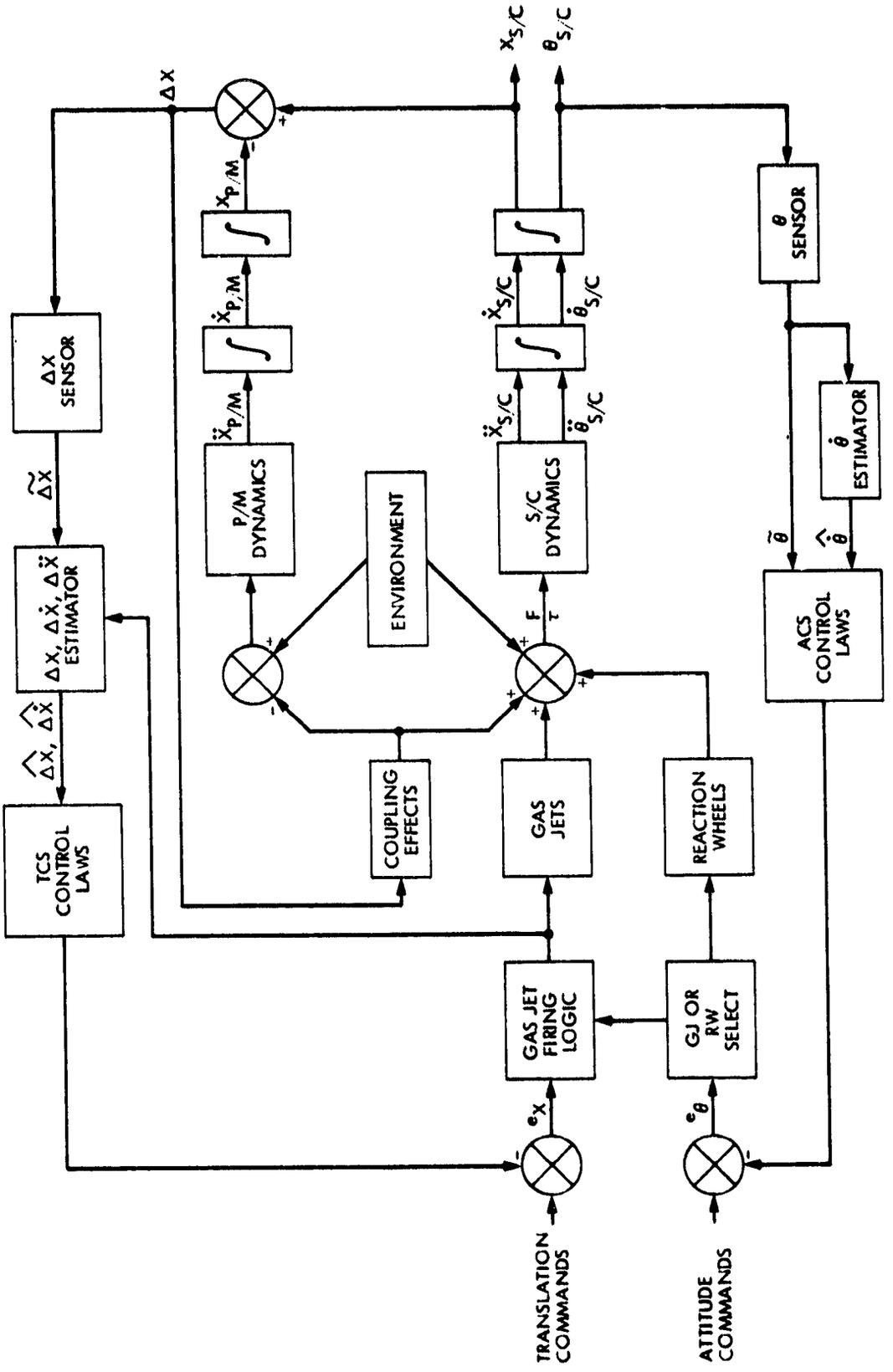

Figure 4. Attitude and Translation Control System Diagram

B. Control System Description

The combined spacecraft attitude and translation control system design shown in Figure 4 includes the inertially referenced dynamics of the proof mass. The spacecraft translation control system is required to track the proof mass motion (i.e. the proof mass solar flyby trajectory) such that the proof mass cavity is centered with respect to the proof mass. This means that translation control will be referenced to the proof mass position, while attitude control will be referenced to inertial coordinates. This combination is acceptable because radiometric telemetry data from the spacecraft can be used to determine its position in inertial coordinates while the translation control system provides the spacecraft position relative to the proof mass. Thus, the proof mass location will be known in inertial coordinates. The primary force that will influence the proof mass and spacecraft trajectories will be solar gravity. In addition to solar gravity the spacecraft will have solar radiation pressure acting on it. The spacecraft will shield the proof mass from the solar pressure so the proof mass trajectory will not be affected by it. Solar gravity and pressure are represented in Figure 4 by the block labeled "environment." Other forces that will influence the spacecraft and proof mass trajectories will be coupling effects which arise from electrostatic charge and self-gravity. These forces will act equally and in opposite directions on the spacecraft and proof mass as shown. The location of the proof mass in its trajectory is shown in the figure as $X_{P/M}$. The summation of solar gravity and pressure forces, coupling forces, and control system forces and torques will determine the spacecraft's trajectory and orientation. Spacecraft location and attitude are shown on Figure 4 as $X_{S/C}$ and $\theta_{S/C}$ respectively. The difference $X_{S/C}-X_{P/M}$ is the position of the spacecraft relative to the proof mass which is labeled

ΔX. This relative position ΔX will determine the size and direction of the coupling forces on the spacecraft and proof mass (this topic is discussed in the subsection on proof mass charge interaction). ΔX will be measured by a capacitance bridge or optical sensor and is shown on the figure as $\widetilde{\Delta X}$ (measured values are indicated by a tilda ~, and estimated values are indicated by a hat ^). ΔX is combined with information about current control system activity (i.e. number and direction of gas jets that are on) and a model of the spacecraft's dynamics to generate estimates of ΔX, $\dot{\Delta X}$, and $\ddot{\Delta X}$. Details about the method and procedure for generating these estimates are given in the subsection on proof mass state estimation. The estimates of ΔX and $\dot{\Delta X}$ are then used in the translation control equations to calculate the translation error. A discussion of translation control equations appears in a later subsection. Translation commands (or bias inputs) appear as part of the translation control design for completeness. Next the summed translation error is evaluated by the firing logic to determine if control action (i.e. firing gas jets) should be taken. The firing logic is also capable of evaluating attitude errors simultaneously, so that a combined but degraded attitude and translation control is possible with just a gas jet system.[+] The firing logic would then enable the appropriate gas jets so as to reduce the control errors.

The attitude control loop is a proportional control design which works independently of the translation control system to maintain attitude stability. The spacecraft attitude can be sensed by sun sensors and star trackers during cruise and by gyros during close encounter. The measured attitude $\tilde{\theta}$ is used by a simple first order filter to estimate the attitude rates. $\dot{\tilde{\theta}}$ and $\dot{\hat{\theta}}$ are then used in the attitude control equations to calculate

the attitude error. The attitude control equations are a rate plus position feedback combination of the form

$$\theta_c = -[(\hat{\theta}_{S/C} - \theta_c) + K_{rp}\hat{\dot{\theta}}] \qquad (3.1)$$

where θ_c is the commanded attitude and K_{rp} is a programmable rate-to-position gain which provides damping to the system and can be selected for optimum performance. The attitude error θ_e which results from this calculation is then directed to a reaction wheel control subloop which in turn applies the appropriate torques to minimize the attitude error. Although a selection of gas jets or reaction wheels can be made, reaction wheels will be the primary attitude control actuators. There will be infrequent intervals, however, that will require gas jets to provide de-saturation of the reaction wheels. This completes the description of the attitude and translation control loops.

+Although the concept of using the canted hydrazine thrusters for both attitude and translation is feasible, it will not satisfy the precision pointing objectives stated earlier. Using only gas jets for control would also heavily cross-couple attitude and translation loops and lead to much more complex limit-cycle control laws for both controllers. Using thrusters for translation control and reaction wheels for proportional attitude control allows these two control functions to be minimally coupled only through any center-of-mass offset from the proof mass cavity center.[8] Thus, the behavior of each function can be made nearly independent of the other, resulting in a less dynamic and more stable spacecraft having the capability to meet all the scientific goals of the STARPROBE mission.

C. Spacecraft Simulation Program

A digital computer spacecraft simulation program (Appendix C) was created for the purpose of studying the control performance achievable with the proposed control system design. This type of computer program is an important analysis tool because it can demonstrate system level performance with respect to changes in any of the three principal elements which influence control performance, (a) the environment to which the spacecraft will be exposed, (b) the spacecraft design, i.e. configuration and mass properties, and (c) the individual components of the control system, i.e. sensors, actuators, on-board computer hardware and software. The modular structure of the program allows the user to make changes in the aforementioned areas by simply substituting more information into the appropriate block of data or calculations. An example of this is the specification of the spacecraft inertia tensor which is the first block of user-specified data in the program (refer to Appendix C). The program version which is listed uses a simple tensor with zero value inertia cross products. If an updated inertia tensor should become available it can be incorporated into the program by substituting the new values including non-zero inertia products. The program has been designed to handle the full 6 degree-of-freedom dynamics problem but may be used for reduced order studies equally as well. To aid the user, most variables and blocks of calculations or data are well annotated in the program. The construction of the program exactly matches the block diagram structure shown in Figure 4. Once this block diagram is understood it is easy to find the corresponding blocks and information flow paths in the simulation program. After the desired models (i.e. sensor, actuator, mass properties, environment, etc.) have been chosen and incorporated into the program the user may select the maneuver

to be simulated. These maneuvers include spacecraft turns on any axis, acquisition of celestial references, or maintenance of steady state pointing and positioning. Maneuver selection gives the analyst several control modes for studying control performance. In addition, the user may specify proof mass and spacecraft initial conditions (positions and rates). Overall the program is very flexible and is easily used to study a wide range of control problems. The program is written in Continuous System Simulation Language in a manner so that someone with minimal computer experience will understand it. Some experience with the JPL UNIVAC computer system is necessary for running the program.

After the program was developed it was first used to study the performance of the on-board proof mass state estimator which is discussed in the next subsection. This was a natural choice for the first set of simulation runs because estimator performance can be investigated with a minimum of program complexity. It is desirable to eliminate all error sources except the estimator from the control system in order to study only estimator performance within the framework of the total system. This was accomplished by using "ideal" models for all of the control system's sensors and actuators except for the ΔX sensor. Simplified models of the environment, spacecraft dynamics, and control laws were also employed to minimize the complexity and cost of conducting the investigation. The program listing which appears as Appendix C is a copy of the program version that was used in the proof mass state estimator performance study.

The simulation program is currently being used to study and develop the translation control laws. For that study the proof mass estimator equations and ΔX sensor model are replaced with idealized

versions so that the translation control performance is solely dependent upon the control laws. The versatility of the program allows the analyst to study not only major system changes (e.g. control with and without a proof mass state estimator) but also parametric changes (e.g. controller and estimator gain variations).

D. Proof Mass State Estimation

The purpose of the proof mass state estimator is to provide accurate estimates of the proof mass position and velocity with respect to the S/C frame. This information is required by the translation control system and the various error compensation models that incorporate proof mass position dependent forces (such as self-gravity and charge disturbances). As this estimation is to be done on board, computational simplicity is an important consideration in the estimator's design.

Initially a Kalman filter based on the full dynamics was designed. This 6-state estimator has the form

$$\dot{\hat{x}} = F(\omega,\dot{\omega},\rho,\dot{\rho},\ddot{\rho})\hat{x} + PH^T R^{-1}(y-H\hat{x}) + u + a_{sp} \tag{3.2a}$$

$$\dot{P} = FP + PF^T + Q - PH^T R^{-1} HP \tag{3.2b}$$

where y is the vector consisting of the three proof mass position measurements, H is the 3 x 6 matrix selecting the observed states (position), $Q = 10^{-4}\text{mm}^2/\text{sec}^3$ diag (0 1 0 1 0 1) is the filter-assumed spectral density of the process disturbance, and $R = 2.5 \times 10^{-5}\text{mm}^2\text{sec}$ diag (1 1 1) is the spectral density of the measurement disturbance.

The sensitivity of the estimator to the arguments of F was exercised by assuming either complete knowledge or no knowledge of these

parameters during a simulated 5° yaw turn. In the first simulation complete knowledge of the parameters was assumed. Furthermore the center of mass was taken to be at the cavity center and stationary. In the second simulation the center of mass was again taken to be stationary, but displaced 10 cm along the z-axis. As this estimator had neither knowledge of this displacement nor knowledge of the angular terms, ω, and $\dot{\omega}$, the arguments of F were set to zero in this simulation. In each simulation a colored noise process disturbance with variance $10^{-4}mm^2/sec^4$ and correlation time of 10 sec was present. Also noisy position measurements (Gaussian, zero-mean, independent, 1σ = .05 mm) were available every 10 milliseconds. The results of the simulations are given in Table 3.1 below.

Table 3.1. Simulation Results for Proof Mass State Estimator

	Average Absolute Error			
Simulation	r_x	$\dot{r}_x$	r_z	$\dot{r}_z$
1	6.16×10^{-3}mm	9.00×10^{-3}mm/sec	8.89×10^{-3}mm	9.32×10^{-3}mm/sec
2	6.23×10^{-3}mm	9.31×10^{-3}mm/sec	8.89×10^{-3}mm	9.31×10^{-3}mm/sec

First note that without filtering the average absolute error in the position measurement would be about .04 mm ($X=N(0,2.5\times10^{-3}mm^2)\rightarrow E|X|\approx.04$ mm). Thus the filter improves the measurement accuracy by more than a factor of four. Next note that there is negligible gain in including the arguments of F into the filter. This is easily explained. Executing the yaw turn results in $|\omega_y|_{max}<2\times10^{-3}$rad/sec and $|\dot{\omega}_y|_{max}<1.25\times10^{-4}$rad/sec^2. Coupling these values with the bounds $|r|\leq 5$mm, $|\dot{r}|<1.5$mm/sec, and $|\rho|<100$mm reveals that the acceleration due to the kinematic terms is less than .01 mm/sec^2 in these simulations. This value is in the noise level, and thus has little

impact on filter performance. We may therefore delete terms in the filter design. This is fortunate in that the estimator (3.2) is fully coupled and time-varying, while the suppression of these terms leads to a decoupled estimator that allows steady state gains (see Appendix B for design).

E. Translation Control Law Development

In Section V of this report translation control concepts such as single-sided limit cycling and integral errors are presented. These concepts were demonstrated using a simple single axis control case. It is shown that these concepts would enable the system to meet the translation control objectives which are to:

(1) Maintain stable spacecraft positioning control relative to the proof mass, and be compatible with attitude control.

(2) Minimize the control gas usage and the number of thruster on/off cycles.

(3) Minimize spacecraft induced disturbances on the proof mass trajectory.

Currently the concepts which were demonstrated for the single axis case are being studied to determine how they apply to the full 3-axis controller. The 3-axis controller has many more constraints than the single axis controller does. One of the most important concerns for the 3-axis controller design will be the effects of having gas jets canted with respect to the spacecraft's principal axes. The heat shield configuration requires that the gas jets be canted. The canted jets will not only require more fuel, (as compared to non-canted jets) but also can result in a further loss of control forces due to plume impingement onto other parts of the spacecraft.

Canted gas jets will also lead to cross-coupled control forces which will drive the deadband limit cycling in a manner that is not yet defined. A better definition of the spacecraft configuration and heat shield design is necessary before the problems of canted gas jets can be fully analyzed. Another concern which arises in the design of the 3-axis controller is how much the attitude and translation control functions are decoupled. If the gas jets alone are used for both attitude and translation control, then realistically these functions cannot be decoupled. The reaction wheel approach avoids having to contend with this severe control problem, and enables compatibility with the previously stated control objectives.

Proof mass charge is yet another major concern in the design of the 3-axis translation control laws. Referring again to Figure 4 it can be seen that the coupling effects of charge will create positive feedback loops around both the proof mass and the spacecraft. (This is obvious because the static charge creates a larger attraction force the closer the proof mass is to the cavity wall.) This destabilizing force is primarily a function of the charge magnitude and the separation distance between the proof mass and the cavity wall. (Refer to section IV for a more complete discussion on proof mass charge effects.) The control system design problem is then to determine how the separation distance should be regulated so as to minimize the destabilizing charge effects and also minimize the amount of control gas expended. If the proof mass were always kept <u>exactly</u> in the center of the cavity then there would be no net charge force and the destabilization problem would never occur. To do this however, would obviously require a much higher control authority, which

implies that a greater amount of control energy must be spent. If minimum fuel expenditure were the only goal then the static charge force would be allowed to drive the proof mass away from a perfect solar gravity trajectory.* However, the control system design must try to minimize both fuel expenditure and proof mass disturbances. The integral control approach discussed in section V.B is one method that offers just such a benefit. Although the integral control concept has been investigated for a single axis model, a 3-axis development has not been done yet. There are several questions that need to be studied before a 3-axis controller can be completely designed: One important question is how should the control strategy for the x and y axes differ from the z axis, since it doesn't seem likely that x and y deadband limit cycling will be single-sided like the z axis. Heat shield asymmetries, thermal warping, and non-nadir attitude will all give rise to x and y axis disturbance forces which cannot be predicted to the same level of confidence as the nominal solar pressure force. Since the signature of these forces cannot be predicted, the translation control design must provide performance that is as insensitive as possible to these disturbances.

No matter what control concept is selected for the 3-axis system there are still other constraints that will influence the control design and performance: One parameter that needs to be studied is the controller bandwidth. This may be a very important parameter if flexible structures are to be attached to the main spacecraft body. Rotating science platforms may also influence the control design since they could create additional disturbances due to mass and momentum unbalances. Any rotating parts may have a momentum vector that will interact with the controller thus making the bandwidth parameter even more important. One other study which must be done to support the controller design is to determine a method for selecting control

gains. Because of the rapid change in solar pressure during the close encounter it may be necessary for the control gains to vary also. It has not yet been determined if time varying or state dependent control gain will be required. If they are required a method for ascertaining the appropriate gains must be developed.

In summary, it is clear that the control system performance must remain relatively constant over a very wide range of disturbance environments. To meet this goal it is evident that several important technology areas still need to be investigated before a 3-axis controller design can be adequately specified.

*It has been proposed to identify the static charge by perturbing the proof mass with a known force and observing its resulting motion. Any uncertainty in the perturbation force will only add to the existing uncertainty about the charge. This would make the problem of controlling the spacecraft with respect to the proof mass even more difficult. In the case of a large perturbation force, or static charge force, the proof mass motion can become too fast for a low bandwidth controller to track (this has been demonstrated using the spacecraft simulation program). This would result in a loss of spacecraft stability relative to the proof mass. It is felt that one of the control objectives must be to minimize the disturbances on the proof mass trajectory caused by charge, even if the magnitude of the charge is unknown or unmeasurable.

IV. DESIGN OF THE PROOF MASS CHARGE ESTIMATOR

Although the proof mass in the drag-free system for Starprobe is shielded from forces external to the spacecraft, there are several factors within the spacecraft environment that can significantly degrade drag-free performance. Among these is an attraction of the proof mass to the cavity shell due to charging of the proof mass. See Appendix E and [7].

A possible solution to this problem is to obtain a reliable estimate of the charge and then include it in the error compensation model. However, this cannot be done a priori since predictability of the exact charge is not possible. This constraint suggests a filtering approach to the problem. To this end a charge force model has been developed ([1],[2]) that describes the motion of the proof mass as a function of charge, the position dependent capacitance of the ball-cavity system, and the plate potentials. (For a complete discussion of the details the reader is referred to Alwar [1].) Incorporating this dynamical description into the disturbance model (32) the charge becomes "observable" through the position of the proof mass.

In this section an extended Kalman filter is developed for the purpose of charge estimation. Also the effect of varying parameters on filter performance is analyzed.

A. The Extended Kalman Filter

Before addressing the specifics of the problem of charge estimation, an overview of the general methodology shall be discussed.

For brevity we shall write the modeled proof mass equations of motion as

$$\dot{r} = f(r,q,t) + w_t \tag{4.1}$$

where r is a 6-dimensional vector representing the position and velocity of the proof mass in the cavity, q is the charge, t is time, and w_t is a white noise process representing a random acceleration. The inclusion of the noise term w_t can improve filter performance in the presence of unmodeled forces [3]. Since this is typically the case when making the transition from a true physical system to a mathematical representation of the system, including such a term is customary.

Now assume q is constant or a slowly varying parameter. We then model q as a Brownian motion and append it to the state x to obtain the augmented state vector $\tilde{x} = \begin{bmatrix} x \\ q \end{bmatrix}$. Thus (4.1) can be rewritten as

$$\dot{\tilde{x}} = \tilde{f}(\tilde{x},t) + \tilde{w}(t) \tag{4.2}$$

where $\tilde{f} = \begin{bmatrix} f \\ 0 \end{bmatrix}$ and $\tilde{w}_t = \begin{bmatrix} v_t \\ z_t \end{bmatrix}$ with z_t the white noise process driving q.

With the capacitive pick-off sensor (or an optical device) the proof mass position is measured. This observation process can be described as

$$y_t = H\tilde{x}_t + v_t \tag{4.3}$$

where y_t is the measured observation, H is a matrix selecting the observed states (position), and v_t is a white noise process representing the accuracy of the measurements. Given the spectral densities of the $\tilde{w}_t$ and v_t processes, say Q and R respectively, equations (4.2) and (4.3) define a filtering problem, i.e., determine the unbiased minimum variance estimate $\hat{x}(t)$ of $\tilde{x}(t)$ given the observations $\{y(s): s \leq t\}$.

The solution to this problem is in general intractable. But in the case that (4.2) is linear i.e. $f(\tilde{x},t) = F(t)\,\tilde{x}(t)$, the solution is given by the Kalman-Bucy filter:

$$\dot{\hat{x}} = F\hat{x} + PH^T R^{-1}(y - H\hat{x}) \tag{4.4a}$$

$$\dot{P} = FP + PF^T + Q - PH^T R^{-1} HP \tag{4.4b}$$

In the problem that concerns us f is nonlinear. However, the linear result above can be applied to this problem by linearizing about a known trajectory. The extended Kalman filter is based upon linearization about the estimated trajectory. The continuous version of these equations is

$$\dot{\hat{x}} = \tilde{f}(\hat{x},t) + PH^T R^{-1} (y - H\hat{x}) \tag{4.5a}$$

$$\dot{P} = \frac{\partial f}{\partial \hat{x}} (\hat{x},t)\, P + P \{\frac{\partial \tilde{f}}{\partial \hat{x}} (\hat{x},t)\}^T + Q - PH^T R^{-1} HP \tag{4.5b}$$

An important feature of the extended Kalman filter is that the gains, $PH^T R^{-1}$, must be computed in real time. This drawback occurs because the covariance equation (4.5b) involves the filtered trajectory $\hat{x}$, which cannot be known a priori.

B. Model Simplification

For completeness the electrostatic force model along the z axis is given below, [1,2].

$$\begin{aligned}
\ddot{r}_z = {} & \varepsilon_o (V_1 - V_3)\{E(V_2+V_4+V_5+V_6) + \tfrac{1}{2} K(V_1+V_3) + \frac{qp}{\varepsilon_o bR} A - \frac{p^2 A}{R} \Big(\sum_{i=1}^{6} V_i\Big)\} \\
& + \frac{r_z}{b} \varepsilon_o \{2F(V_1+V_3)(V_2+V_4+V_5+V_6) + 2\,G(V_2+V_4)(V_5+V_6) \\
& + 2\,I\,V_1V_3 + 2J(V_2V_4+V_5V_6) + L(V_1^2+V_3^2) \\
& + \frac{p^2 N}{R} \Big(\sum_{i=1}^{6} V_i\Big)^2 + \frac{q^2}{(\varepsilon_o b)^2} \frac{N}{R} + M(V_2^2+V_4^2+V_5^2+V_6^2) \\
& + \frac{2Q}{\varepsilon_o b} \frac{p}{R} (B(V_1+V_3)+D(V_2+V_4+V_5+V_6)) - \frac{2q}{\varepsilon_o b} \frac{PN}{R} \Big(\sum_{i=1}^{6} V_i\Big) \\
& - \frac{2p^2}{R} (B(V_1+V_3)+D(V_2+V_4+V_5+V_6)) \Big(\sum_{i=1}^{6} V_i\Big) - \frac{p^2 A^2}{R} (V_1-V_3)^2\} \\
& + \frac{r_y}{b} \varepsilon_o (V_1-V_3)(V_2-V_4) \{H - \frac{p^2 A^2}{R}\} \\
& + \frac{r_x}{b} \varepsilon_o (V_1-V_3)(V_5-V_6) \{H - \frac{p^2 A^2}{R}\}
\end{aligned} \tag{4.6}$$

where q = charge, V = potential on i^{th} plate, and the other terms are known constants derived from the configuration of the drag-free sensor. To deduce the charge from proof mass motion this model must be inserted into the disturbance model. The resulting equations of motion simplify considerably under the following assumptions:

(1) the center of mass of the S/C is fixed,

(2) the S/C angular rates are zero,

(3) the plate potentials on the z-axis are of equal magnitude and opposite sign, and the remaining plates are grounded.

The first two assumptions allow us to set the basic requirements for charge estimation - voltages on plates, accuracy of measurements, level of charge, etc. Once bounds on these parameters are established, then we can proceed with the analysis of introducing S/C angular rates and a non-stationary center of mass. The third assumption, although a matter of convenience, is easily justified by noting that the force due to charge along any given axis is independent of the other axes. Hence, the charge is not observed through the coupling terms, and consequently this assumption has no impact on estimator performance.

C. Filter Design

With the assumptions above, (4.6) conveniently decouples and it is sufficient to consider the dynamics along the z-axis

$$\ddot{r}_z = \frac{2V(t)q\ pA}{mbR} + \frac{\varepsilon_o}{mb}\left[V^2(t)\ \left(2L - \frac{4p^2A^2}{R}\right) + \frac{q^2N}{\varepsilon_o^2 b^2 R}\right] r_z + u(t) + a_{sp} + f_d \quad (4.7)$$

where

r = displacement (meters)

q = charge (coulombs)

V(t) = potential (volts)

ε_o = permittivity of free space (8.854×10^{-12} farads/m)

m = mass of proof mass (.2 kg)

a = radius of proof mass (.011 m)

b = radius of cavity (.020 m)

u(t) = modeled control law (see sec. III)

u = modeled acceleration due to solar pressure (10^{-4}m/sec^2)

f_d = sum of unmodeled/mismodeled accelerations,

and, corresponding to a/b = .55 (see [1])

A = 3.317

L = 6.424

N = 1.466

p = 1.203

R = 15.36

Since the disturbance term f_d in (4.7) is unknown, in the filter design it is replaced by a white noise process w_t (recall that this is required for stability of the steady state filter). With the assumption that q is constant over small time durations (500 seconds), the filter will be designed from the dynamics

$$\dot{x}_1 = x_2 \tag{4.8}$$

$$\dot{x}_2 = \frac{2V(t)q\ pA}{mbR} + \frac{\varepsilon_o}{mb}\left[V^2(t)\ \left(2L - \frac{4p^2A^2}{R}\right) + \frac{q^2N}{\varepsilon_o^2 b^2 R}\right]x_1 + u(t) + a_{sp} + w_t$$

$$\dot{q} = 0$$

and the observations

$$y = x_1 + v \tag{4.9}$$

where $x_1 = r_z$, $x_2 = \dot{r}_z$, and v_t is again a white noise process reflecting measurement uncertainty.

Note that (4.8) is nonlinear. Thus we shall make use of the extended Kalman filter. Let Q and r denote the spectral densities of the $[0\ w\ 0]^T$ and v processes respectively. Then making the appropriate substitutions into (4.5a) and (4.5b), the extended Kalman filter for this problem is

$$\begin{bmatrix} \dot{\hat{x}}_1 \\ \dot{\hat{x}}_2 \\ \dot{\hat{q}} \end{bmatrix} = \begin{bmatrix} \hat{x}_2 \\ \frac{2V(t)\hat{q}\ pA}{mbR} + \frac{\varepsilon_o}{mb}\left[V^2(t)\ \left(2L - \frac{4p^2A^2}{R}\right) + \frac{\hat{q}^2N}{\varepsilon_o^2 b^2 R}\right]\hat{x}_1 + u(t) + a_{sp} \\ 0 \end{bmatrix} + \frac{1}{r} P \begin{bmatrix} 1 \\ 0 \\ 0 \end{bmatrix} (y - \hat{x}_1) \tag{4.9a}$$

$$\dot{P} = \begin{bmatrix} 0 & 1 & 0 \\ f_{21} & 0 & f_{23} \\ 0 & 0 & 0 \end{bmatrix} P + P \begin{bmatrix} 0 & f_{21} & 0 \\ 1 & 0 & 0 \\ 0 & f_{23} & 0 \end{bmatrix} + Q - \frac{1}{r} P \begin{bmatrix} 1 & 0 & 0 \\ 0 & 0 & 0 \\ 0 & 0 & 0 \end{bmatrix} P \tag{4.9b}$$

where

$$f_{21} = \frac{\varepsilon_o}{mb}\left[V^2(t)\ \left(2L - \frac{4p^2A^2}{R}\right) + \frac{\hat{q}^2N}{\varepsilon_o^2 b^2 R}\right]$$

$$f_{23} = \frac{2V(t)\ pA}{mbR} + \frac{2\hat{q}N}{\varepsilon_o^2 b^2 R}\hat{x}_1$$

Before proceeding with a discussion of filter performance, some general remarks on the structure of this filter are in order.

The need for resorting to an extended Kalman filter for charge estimation arises because of the nonlinearity introduced by q^2 in (4.8). If this term did not appear, then the filter constructed above would reduce to the ordinary Kalman-Bucy filter. Furthermore, if we have the following strong inequality

$$\left|\frac{q^2N}{\varepsilon_o^2 b^2 R}\right| << V^2(t)\left[2L - \frac{4p^2A^2}{R}\right], \left|\frac{2V(t)q\ pA}{mbR}\right| \qquad (4.10)$$

(i.e. when the significance of the nonlinearity diminishes), we would expect the performance of the extended Kalman filter to be similar to that of a Kalman-Bucy filter designed without knowledge of the q^2 term.

Now suppose (4.10) holds and consider the Kalman-Bucy filter just described. By adding a noise term in the model dynamics for q (equation (4.8)), it was determined that the resulting Kalman-Bucy filter is uniformly completely controllable and observable. Moreover, since the model errors are bounded (the deleted q^2 term is included here now), it can further be shown that the true covariance of the state estimate is uniformly bounded [3].

The conclusion from this is that we are reasonably assured that the extended Kalman filter will "work" in some fashion, i.e. the estimated state will not diverge from the true state.

D. Simulations, and Analysis of Results

The parameters exercised in the simulations include charge, observation noise, process noise (disturbances), and plate potential amplitude and frequency. As only one proof mass-cavity configuration was used, the capacitance coefficients and the proof mass radius and mass were fixed in the simulations.

Below we give the range of magnitudes these parameters were allowed to take, and the rationale behind the choice.

Two values of charge were selected to be estimated, 10^{-11} coulombs and 10^{-10} coulombs. The first value is near the bound at which the charge begins to degrade drag-free performance (i.e. producing accelerations

greater than 10^{-9} m/sec^2), while the second value represents an a posteriori upper bound on the charge for the filter to be viable (we'll get to this later).

In each of the simulations it was assumed that noisy proof mass position information was available every 10 milliseconds. It was further assumed that the sensor noise was zero-mean, Gaussian, and independent. Standard deviation values of 5μ and 50μ were chosen to exercise this parameter. These values are in the range of realistic displacement sensor resolution.

The process noise reflecting the unmodeled/mismodeled disturbances was always taken to be a stationary, exponentially correlated Gaussian process. The time constant of the process was varied between 10 sec and 50 sec, and the variance of the process was varied between $100\mu^2/\text{sec}^4$ and $2500\ \mu^2/\text{sec}^4$. The reasoning here stems from the anticipation that a major contributor to the disturbance f_d will be a mismodeled (non-steady component) solar pressure. Thus the variances reflect the assumption that the disturbance magnitude is between 10% and 50% of the modeled solar pressure. The choice of time constants expresses the belief that the dynamics occurs at low frequencies associated with attitude motions and heat shield asymmetries or surface irregularities.

The proof mass was excited by a square wave potential in each simulation. This choice is useful for charge estimation in that a "dither" due to the charge effect is superimposed on the proof mass trajectory at a known frequency. Presumably if this frequency is sufficiently isolated from the effective frequencies of the unknown disturbances, then the estimate of charge will not be seriously degraded by these disturbances.

The frequencies selected ranged from .05 hz to .5 hz, and the potentials ranged from 250 v to 1000 v. These values were driven to a great extent by the other parameters.

Given a particular set of parameters, observations were generated via equations (4.7) and (4.9). The filter designed for a set of parameters was obtained via equations (4.8) and (4.9), with $r = \frac{\sigma^2 sec}{100}$ (σ = 1 standard deviation of measurement noise) and $Q = 100\mu^2/sec^3$. The initial estimate of the charge was always taken to be zero. Also the initial variance $P_{33}(0)$, was selected so that $3\ q^2 = P_{33}(0)$.

Before examining the specifics of the analysis, a criterion for judging estimator performance is necessary.

Recall that the drag free objective is to assure that unmodeled accelerations on the proof mass do not exceed $10^{-9} m/sec^2$. From equation (4.7) it follows that the acceleration due to charge alone (i.e. when v = 0) is

$$\frac{q^2 N}{\varepsilon_o^2 mb^3 R} |r_z| \tag{4.11}$$

Thus to guarantee that the absolute difference between the estimated and actual acceleration is less than $10^{-9} m/sec^2$, it is necessary that

$$|q-\hat{q}| \leq \frac{10^{-9} \varepsilon_o mb^3 R}{|r_z|\ |q+\hat{q}|N} \sim \frac{1.5 \times 10^{-25}}{|r_z|\ |q+\hat{q}|} \tag{4.12}$$

with the inequality above in mind, we create three categories for ranking filter performance. They are:

Category A - Estimator satisfies (4.12) with $|r_z| = 4.5 \times 10^3$ m over the last 50 sec. of the run.

Category B - Estimator satisfies (4.12) with $|r_z| = 2.25 \times 10^{-3}$ m over the last 50 sec. of the run.

Category C - The complement of categories A and B.

These rankings basically give a measure as to how narrow the deadband in the translation control system must be set to attain the required drag free performance.

An unfortunate ramification of (4.12) is that the greater the charge, the more precise the estimate needs to be. To put this into perspective, assume an actual charge of 5×10^{-12} coulombs is to be estimated. In this case an estimate of 0.0 is acceptable. On the other hand if the value of the charge is 10^{-9} coulombs, then it would be necessary for the estimate to be within 10^{-14} coulombs.

The simulations that were performed are presented in Table 4.1.

We shall first investigate the results of the simulations involving a charge of 10^{-11} coulombs. Substituting into (4.12) we find that the estimate $\hat{q}$ must satisfy

$$\left.\begin{matrix} 8.2 \times 10^{-12} \\ 5.8 \times 10^{-12} \end{matrix}\right\} < \hat{q} < \begin{cases} 1.15 \times 10^{-11} & \text{- category A} \\ 1.29 \times 10^{-11} & \text{- category B} \end{cases} \tag{4.13}$$

Note that only one simulation (#6) at the lower voltage made the A category. This is not surprising since a higher voltage results in a greater "dither" of the proof mass. The role of the voltage and frequency is most readily observed in the propagated variances. These variances reflect how well the filter "thinks" it is performing. It is apparent from Table 4.1 that higher voltages and/or lower frequencies result in smaller variances. Now since the acceleration due to the quadratic charge term is <u>independent</u> of these parameters, we are led to conclude that the bulk of the identification is done through the linear charge term. This too is not surprising, since with this set of parameters (V=250 - 1000 $q=10^{-11}$ coulombs) the q acceleration dominates the q^2 acceleration by 2-3 orders of magnitude.

Table 4.1. Simulation Results for Charge Estimation

Run#	Charge	Voltage	Frequency	Observation noise 1σ	Process noise(1σ, corr./time)	Terminal Variance*	Rank
1	10^{-11}coul	1000v	.5 hz	5μ	10μ , 10 sec	1.76×10^{-23}coul^2	A+
2	"	"	.1 hz	"	" , "	1.24×10^{-23}coul^2	C
3	"	"	.05hz	"	" , "	1.21×10^{-23}coul^2	C
4	"	"	.1 hz	"	" , 50 sec	1.24×10^{-23}coul^2	C
5	"	"	.2 hz	"	" , 25 sec	1.34×10^{-23}coul^2	A
6	"	250v	"	"	" , "	1.78×10^{-22}coul^2	A-
7	"	1000v	"	"	50μ, "	1.34×10^{-23}coul^2	B
8	"	"	"	50μ	10μ, "	2.30×10^{-23}coul^2	B
9	"	250v	.5 hz	5μ	10μ, 10 sec	2.23×10^{-22}coul^2	B+
10	"	1000v	"	50μ	" , "	2.58×10^{-22}coul^2	B-
11	"	"	.2 hz	5μ	" , 10 sec	1.34×10^{-23}coul^2	A
12	"	"	.5 hz	"	100μ, .005 sec	1.76×10^{-23}coul^2	B-
13	10^{-10}coul	"	.2 hz	"	10μ, 25 sec	1.35×10^{-23}coul^2	B
14	"	"	"	50μ	" , "	2.32×10^{-23}coul^2	C
15	"	250v	"	5μ	" , "	2.09×10^{-22}coul^2	C

*This is the filter propagated variance, not the actual variance.

Next, note that none of the simulations with observation noise of 50μ made the A category. This can be explained by the following argument.

Focusing now on the q-term, since this is what the filter primarily responds to, a quick computation yields $\frac{1}{mbR}\ |2VqPA| \approx 1\mu/sec^2$ (for V=1000). Therefore over a period of T seconds in which V = constant, the perturbation ΔZ, due to this acceleration is approximately

$$\Delta z = \frac{1}{2\Gamma^2}\left[e^{\Gamma T} + e^{-\Gamma T} - 1\right] \quad \text{(microns)} \tag{4.14}$$

where

$$\Gamma = |V| \sqrt{\frac{\epsilon_o}{mb}\left(2L - \frac{4P^2A^2}{R}\right)} \approx .14$$

Taking T = 2.5 sec, we get a "dither" amplitude of about 3.15 μ. Obviously a 50μ resolution displacement sensor is going to run into a sensitivity problem here since the motion is down at the 1/15σ level. This problem however, does not occur with a 5μ sensor.

Referring to (4.14) we see that increasing V or T results in an exponential increase in the dither. Although increasing the voltage would significantly enhance the identification, the trade-off in the translation control performance quickly becomes intolerable (see Sec. III). The alternative then is to decrease the dither frequency. Unfortunately this too has its drawbacks - which brings us to the role of process noise.

The parameters of the disturbance were exercised in simulations 2, 4 and 7. The results indicate a great sensitivity to the correlation time of the process, and a lesser sensitivity to the variance of the noise process.

Loosely speaking, the failure of the filter in these simulations can be attributed to the disturbance having too much power at the dither frequency. It is easy to see how the filter breaks down in this case. The acceleration due to charge is approximately $1\mu/sec^2$, while the disturbance

is one order of magnitude greater. Obviously, if the disturbance has substantial spectral content at the excitation frequency convergence will be slow, and not necessarily to the correct value. The following "worst case" example illustrates this point.

Suppose the disturbance, f_d, and the plate potentials are both constant. In this case the effect of the charge is virtually indistinguishable from the disturbance. As a result the filter will attribute the disturbance to the charge. Now when the charge is constant or slowly varying the filter believes it learns its value very well. Consequently, the relative error in the estimate will be $|f_d|/1\mu sec^2$.

Based on the simulation results (where $f_d = 10\mu/sec^2$, 1σ value) and the example above, it is clear that "dithering" substantially reduces estimation errors due to mismodeling.

So on the one hand we would like the dither to be fast to reduce model errors, while on the other hand we require it to be slow enough to be visible to the sensor.

There are a few other deductions that can be made from the illustration above. To this end rewrite equation (4.7) as

$$\ddot{r}_z = k_1 Vq + k_2 V^2 r_z + f_d \qquad (4.15)$$
$$\dot{q} = 0$$

Note that the disturbance now incorporates the quadratic charge term. Suppose a Kalman-Bucy filter is derived for this dynamical system (with f_d replaced by a white noise disturbance model and the same observation process in (4.9)). It is not difficult to show in this case that the variance in the charge estimate $P_{33}(t) \to 0$ as $t \to \infty$. We would therefore anticipate the terminal variances to be near zero. This, however, was not the case. The terminal variances were in the 1.3×10^{-23} to 2.4×10^{-22} coulomb range,

less than two orders of magnitude under the initial variance. Although it may be argued that the covariance in the extended Kalman filter is coupled to the state estimate (while the Kalman-Bucy filter is not), and hence susceptible to model errors, it was found that the principal drivers of the variance were the parameters independent of the disturbance - voltage, dither frequency, and observation noise. (And as to be expected, higher voltage, slower dither, and better observations produced smaller variances.) Furthermore, a white noise simulation (#12) produced errors consistent with the propagated variance (1σ error $\approx 4 \times 10^{-12}$ coulombs). From this we conclude that the filter believes it needs more time to converge, i.e., it is still sensitive to new observations after 500 seconds.

Convergence can be hastened by increasing V, decreasing R, or decreasing Q. If we choose to have the filter conform to the model, the first two possibilities are out of the question by virtue of previously discussed constraints. This leaves us with the selection of the spectral density Q, which is essentially a reflection of how much the model deviates from reality. Thus not only is the filter sensitive to model errors, it is also sensitive to its perception of these errors.

The obvious conclusion to be drawn here is that given the existing constraints on plate potentials and sensor resolution, a more thorough understanding of the disturbance environment is needed. A cursory analysis of the problem is given in Appendix A.

One other deduction can be made based on the analysis stemming from the model (4.15) - the extended Kalman filter is superfluous at this magnitude of charge. This follows from the observation that the extended Kalman filter requires a dither acceleration of 1μ/sec^2, while the acceleration due to the

quadratic term in charge is

$$\left| \frac{q^2 N}{\varepsilon_o^2 m b^3 R} r_z \right| \leq 10^{-2} \mu/sec^2$$

Thus according to previous arguments, neglecting the quadratic term will contribute less than 1% error in the estimate. And discarding this term is equivalent to replacing the extended Kalman filter with a Kalman-Bucy filter.

All of the analysis above pertains to the case where $q = 10^{-11}$ coulombs. The situation changes significantly for increasing charge levels. This is due to the tightening of the error requirement (4.12). Whereas an 18% error is tolerable at 10^{-11} coulombs, the requirement drops to .18% at 10^{-10} coulombs.

No simulation achieved this level of performance. Simulation 13 stayed within an approximate .3% band of the actual value, while simulations 14 and 15 were in a 1% - 2% range. Using a ranking system that is equivalent to the rankings for the simulations run at 10^{-11} coulombs, we find that simulation 13 is a marginal "B", and simulations 14 and 15 are unequivocal "C"'s.

One noteworthy aspect of these simulations is that the terminal variances were in the same range as the variances in the previous simulations. Thus there was 3-4 orders of magnitude decrease from the initial variance. This is not entirely surprising since we had earlier anticipated the stability of the filter, which implies that the initial statistics are forgotten.

An extremely important element in all the simulations was the assumption of perfect knowledge of the voltage. Errors in this knowledge propagate two types of disturbance compensation errors. First, a bias in the estimate of the voltage will yield a proportional error in the charge

estimate. As we have seen with increasing charge values, this type of error can quickly become disastrous. The second type of error, that presents a potentially greater problem, is the actual S/C trajectory error introduced by the V^2 term. Recalling that we have essentially set a requirement of V = 1000 volts to identify the charge, the acceleration due to this potential is

$$\frac{\varepsilon_o}{mb} V^2 \left[2L - \frac{4p^2A^2}{R}\right] (4.5 \times 10^{-3}) \approx 8.6 \times 10^{-4} \text{m/sec}^2 \qquad (4.16)$$

Thus to ensure an error of less than, 10^{-9}m/sec^2 we need

$$|V - \hat{V}| \approx 10^{-3}V \ . \qquad (4.17)$$

Integral control can compensate for this error to some extent. But needless-to-say, a closer look at this problem will be necessary.

V. INTEGRAL CONTROL

A. Rationale for Integral Control Disturbance Reduction

During close encounter, solar pressure will be the dominant non-gravitational force acting on the spacecraft. Furthermore, since the spacecraft is nadir pointed, the solar pressure will be in a constant direction in spacecraft coordinates. As a result, the translation control system will be operating in a nearly single-sided limit cycle along the z axis.

A proportional control system (the continuous approximation of the on-off control system) acting on the second order spacecraft dynamics in the presence of a constant disturbance will produce a constant proof mass position offset. Consequently, the proof mass will spend a larger portion of its time on the -z axis than it will on the +z axis.

Any mechanism for producing a proof mass disturbance due to a constant proof mass offset will thus be enabled through the critical

perihelion passage. Proof mass charge and self-gravity are two such mechanisms.

There exist several methods for minimizing proof mass disturbances due to charge and self-gravity. Since some proof mass disturbances result from the proof mass not being centered in the cavity, one approach is to reduce the proof mass travel range by "tightening" the drag-free control system. In theory, this may be accomplished by expending a great deal more control fuel.

A second approach is to permit larger excursions of the proof mass while monitoring both the proof mass charge, and the vehicle mass distribution. This allows for real time computation of the proof mass disturbances, effects which can then be included in the drag-free trajectory estimation. However, a difficulty arises in trying to monitor the proof mass charge.

The charge "identification" procedure requires some type of proof mass forced vibration or dither; the larger the response of the proof mass to the known dither, the greater the proof mass charge. In order to make the proof mass response visible to the existing proof mass sensor system, a sizable force must be applied to the proof mass. Although this force is "known," the relative precision to which it must be known increases as the magnitude of the identification force increases. The accuracy to which the adverse effects of the charge identification procedure can be removed will depend upon the applied force knowledge.

Integral control is the traditional appoach to minimizing the effects of constant disturbances. As applied to drag-free control, a very low bandwidth integral control term can be added to the present drag-free control scheme. Because the integral effect is low bandwidth, there will be very little interaction with the basic drag-free control dynamics. The

integral term will keep the proof mass at the center of the cavity on the average, rather than slightly biased, as a proportional system would do. Very little additional control fuel should be required for this scheme, and, additionally, the proof mass is not disturbed. There is also some degree of adaptability to an unknown magnitude of solar pressure force. The modification of the single-sided drag-free control law using integral control will be the topic of the next section.

It should be noted that in theory two levels of integral control are required to eliminate the proof mass disturbance due to charge. The proof mass disturbance force is, to first order, proportional to the proof mass position. Therefore double integral control of the proof mass position is the control that will produce zero proof mass trajectory error. Double integral control is a topic for future study.

B. Integral Control Model

Near the sun, the external disturbance environment is accurately described by a constant force due to solar pressure, in addition to a small random component. As a result, a single-sided limit cycle is appropriate for control purposes. In this limit cycle, the thrusters are essentially firing occasionally to negate the effects of the opposing solar pressure drag. A phase plane plot of the single-sided limit cycle is shown in Figure 5.1.

In other words, after the proof mass motion relative to the spacecraft has accumulated a net positive velocity, and is in the positive x direction (A), the thruster fires. The thruster eventually reverses the proof mass velocity (B), and the proof mass begins to drift in the negative

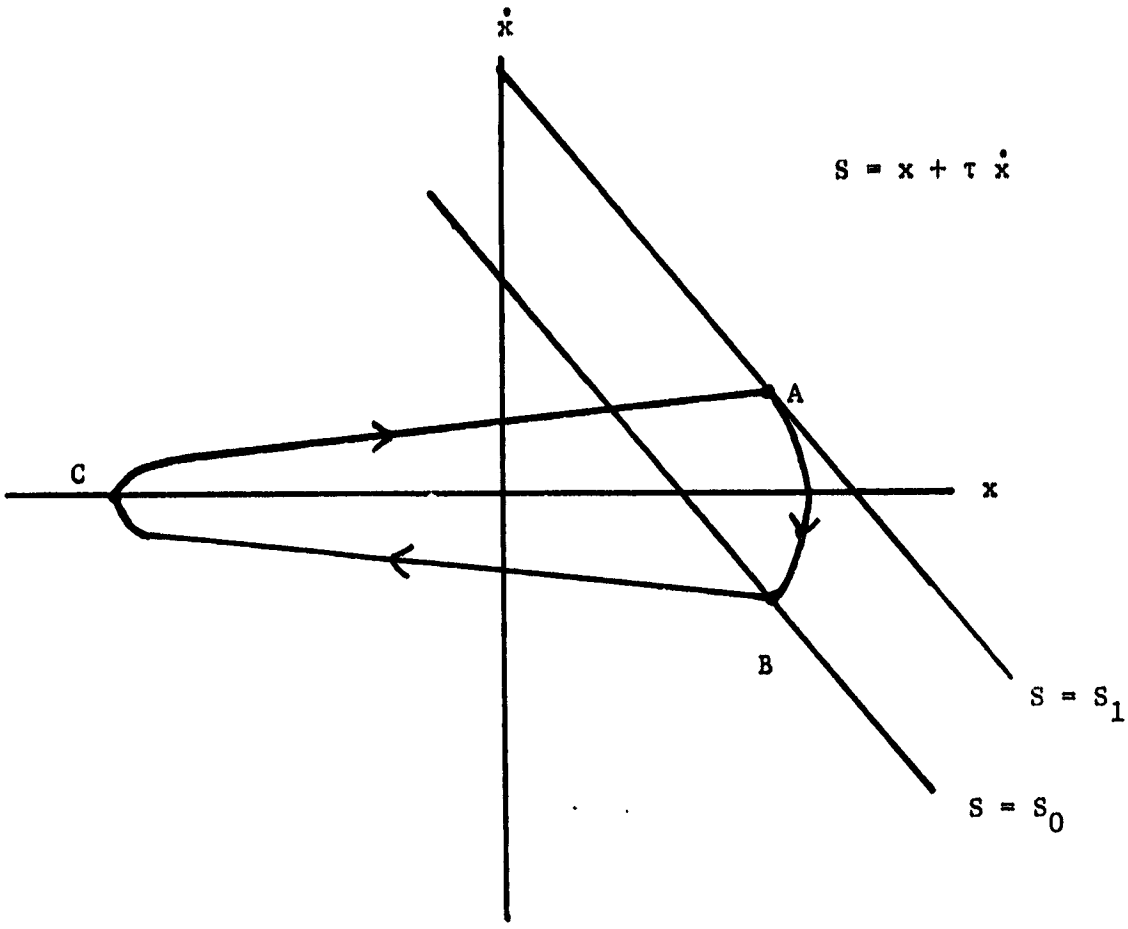

Figure 5. Phase Plane Plot of Single-Sided Limit Cycle.

x-direction. The relative speed of the proof mass is gradually reduced by the solar pressure until it reaches its maximum negative excursion (C), and then, the solar pressure further accelerates the proof mass back to A.

Maximum use of the proof mass housing size can be realized by making the maximum positive excursion, x^+, and the maximum negative excursion, x^-, equal in magnitude, and as large as possible without allowing the proof mass to touch the housing. As might be expected, however, the maximum negative excursion (C) is highly dependent upon the magnitude of the solar pressure at a particular point in orbit, and is not likely to be well known a priori. Even if this problem could be circumvented, there is yet an additional problem. For the case where x^+ and x^- are equal in magnitude,

the proof mass average position in the limit cycle is not at the center of the cavity (just as a bouncing ball's average position is not at 1/2 its maximum height).

The modified control law includes an integral control term. The purpose of this term is to keep track of the integrated position error, and to adjust the thruster-off switch line to asymptotically reduce the integral of the proof mass position offset to some small bounded value. This scheme is adaptable to a wide range of disturbance environments, alters the single-sided limit cycle only slightly, uses roughly the same fuel, is easy to implement, and maintains the integral of the proof mass offset to a small level.

The integral controller is composed of two parts; first, a part that keeps track of the integral error, and second, logic that incorporates the integral error information in commanding the thrusters. The first component is easily constructed. Since a position measurement is already available from the proof mass sensor, a simple integrator (amplifier, capacitor, resistor) is all that is required to keep track of the integrated position offset. A discussion of what to do with this position integral information follows.

The integral control to be added can be low bandwidth, since reducing the effects of charge and self-gravity requires the proof mass integral position error to be small "on the average." As such, the basic structure of the single-sided limit cycle will be retained, with corrections to account for the integral error term being made only every few cycles. By keeping the thruster-on switch line as in Figure 5.1, it is fairly certain that the proof mass will never touch the positive wall. The technique behind the integral control action is to monitor the value of the integral error once

per cycle, and to adjust the thruster-off switch line slightly so as to eventually bring the integral error to the desired value.

Certainly, the desired integral error term can be chosen, and the current value of the integral error can be updated. The only additional piece of information needed to eventually achieve the desired integral error value is the average integral error accumulated per cycle as a function of switch-off line value. This calculation is given below.

Define the following parameters.

S_1 is the value of the switch on line

S_0 is the value of the switch off line

τ is the slope of the switch line

A_c is the magnitude of the control acceleration

A_d is the magnitude of the disturbance acceleration, and

$x^+(x^-)$ is the maximum positive (negative) proof mass position

Since the position of the proof mass as a function of time is parabolic, the average position is given by 2/3 of the maximum value of the parabola. These values for the thruster-on and the thruster-off must then be weighted in proportion to the duration of the thruster-on and thruster-off times, respectively. It is easily shown that

$$x^+_{avg} = 1/2\ (S_1 + S_o) + 1/6\ \frac{(S_1-S_o)^2}{(A_c-A_c)\tau^2}$$

$$x^-_{avg} = 1/2\ (S_1 + S_o) - 1/6\ \frac{(S_1-S_o)^2}{A_d\ \tau^2} \qquad (5.1)$$

and, the thruster on and thruster-off times are given by

$$T_{on} = \frac{S_1-S_o}{(A_c-A_d)\tau}\ ,\ T_{off} = \frac{S_1-S_o}{A_d\tau} \qquad (5.2)$$

The averaged integral error accumulated per cycle, I, is then simply

$$I = \frac{x^+ T_{on} + x^- T_{off}}{T_{on} + T_{off}} \tag{5.3}$$

After some algebra, the following result is obtained

$$I = \frac{S_1+S_o}{2} + 1/6 \frac{(S_1-S_o)^2}{\tau^2} \left[\frac{1}{A_c-A_d} - \frac{1}{A_d}\right] \tag{5.4}$$

Solving for S_o in terms of the desired value of the integral error, I_d, and the current value of the integral error, I,

$$S_o = \frac{-B + \sqrt{B^2 - 4 * C * (S_1^2 C + S_1 + 2(I_d-I))}}{2C} \tag{5.5}$$

where $C = \frac{1}{3\tau^2} \left[\frac{1}{A_c-A_d} - \frac{1}{A_c}\right]$, and $B = 1-2\ CS_1$

Equation (5.5) shows that if a desired value of the integral error is given, and if the current value of the integral error is known, then the switch-off line S_o can be computed.

The "bandwidth" of the integral control can be easily adjusted by correcting only a fractional change of I at each cycle (say 1/10) instead of the full value.

C. Simulation and Discussion of Results

A computer program was developed for simulating one dimensional proof mass motion in the housing using the single-sided limit cycle with

integral control. The values of the parameters chosen for one particular run were

S_1 = 3.1 mm

S_0 = 1.9 mm

τ = 0.20 sec

A_c = 3.3 mm/sec^2

A_d = 1 mm/sec^2 $\approx 10^{-4}$g (at least three times higher than the expected solar radiation effect)

I_d = -30 mm-sec

The proof mass diameter was assumed to be 22 mm and the housing diameter was assumed to be 40 mm. Also, a random acceleration component of 0.05 mm/sec^2 with a correlation time of 0.1 sec was assumed to be present. The results of the simulation for 260 cycles (about 1895 sec) yielded

x^+ = 6.479 mm

x^- = -6.605 mm

I_{max} = +8.213 mm sec

I_{min} = -43.709 mm sec

fuel usage = 2740 mm/sec (equivalent velocity increment)*

These results indicate that the integral controller performed quite well. The maximum positive and negative excursions of the proof mass were roughly symmetric with respect to the cavity center, used a substantial portion of the cavity space, and were still bounded well away from the cavity walls.

The integral error remained bounded (rather than growing indefinitely without the integral control term) within a very small range. Note that a 44 mm-sec position integral error over the 1900 sec simulation time

corresponds to an average proof mass position of 44 mm-sec/1900 sec or 0.023 mm from the cavity center! This is the benefit of the integral control term. The total velocity increment applied to the spacecraft by the constant solar pressure term was 1895 mm/sec. It should be noted that no additional control fuel was required to compensate for the random component of the solar pressure model, while at the same time, performing the drag free control function with integral control.

*For a 1,000 kg spacecraft, the mass of hydrazine propellent required in the 1/2 hour period is approximately 1.5 kg using an A_d value of 10^{-4}g.

VI. KEY CONCLUSIONS AND FUTURE STUDIES

The preceding sections have provided discussions of the major areas investigated in the on-board estimation and control synthesis of a drag-free system for the Starprobe Mission and Spacecraft. These studies, along with the supporting appendices and references, have taken a major step towards the system definition and understanding of functional requirements.

Analysis techniques and simulation programs have been developed to explore important issues identified in earlier feasibility studies [4,5,6]. The basic attitude and translation control system topology has been expanded to a full six degree-of-freedom simulation framework with dynamical and environmental cross-coupling linkages. Translation state estimation and proof mass charge estimation have been analytically developed, and parameter constraints have been identified and quantified. An integral-error control technique has been applied to the problem of identifying and measuring proof mass disturbances. This should provide a particularly important complement to the charge estimation approach, in that integral error control

can reduce the effects of charging on the proof mass trajectory resulting from translation limit-cycle non-symmetry during solar encounter.

The sensitivity of the proof mass translation state estimator to angular rates and accelerations of the spacecraft was determined for a simulated 5 degree yaw turn (or imaging slew). Simulating the 0.1 degree/sec slew revealed that the acceleration due to the kinematics with a center-of-mass offset of 10 cm from the cavity center is less than 0.01 mm/sec^2. This magnitude was shown to have little impact on the filter performance; therefore, the reaction wheel controlled angular rate and acceleration terms may be deleted in the filter design. The major benefit of this is to allow a decoupled estimator with steady state gains to be realized - a most important asset for on-board implementation.

In the charge estimator synthesis a set of rather specific constraints have been found within which the estimator performs at an acceptable level of accuracy and convergence. These parameter constraints are:

(1) A proof mass charge magnitude in the range of 10^{-11} coulombs, or less.

(2) Capacitive plate potentials of 1 Kv.

(3) An identification dither frequency sufficiently removed from disturbance frequencies, yet low enough to ensure visibility to the proof mass displacement sensor, i.e., 5 Hz or less for sensor visibility.

(4) A proof mass displacement sensor resolution of 5 microns (0.005 mm).

The analysis has established filter sensitivity to unmodeled/mismodeled disturbances. We would expect that as a better disturbance model develops some of the above constraints might be relaxed. In particular,

if an improved model allows for a decrease in dither frequency then a lower voltage or a noisier sensor may be tolerated.

Within these constraints the likelihood has emerged that a Kalman-Bucy filter would be as effective as the extended Kalman filter for charge estimation. The clear advantage of the Kalman-Bucy form is the simplicity of precomputed gains, thus making it amenable to on-board implementation.

While the accomplishments of the work to date are significant there remains a considerable task ahead in the areas of requirements definition and system analysis. A brief discussion of these future study needs and a realistic perspective on the critical issues is given in what follows:

Although the integral control concept has been investigated with a single axis model and found to be quite promising, a three-axis development is needed. There are several issues that need to be studied before a complete controller can be properly specified and designed. An important question to address is how should the control technique for the transverse (X and Y axes) differ from the longitudinal (Z) axis since it is unlikely that transverse limit cycles will be single sided like the Z axis. Heat shield asymmetries, thermal warping, and non-nadir pointing/perturbations will give rise to transverse axis disturbances very difficult to predict. Since the signatures of these forces cannot be adequately known (magnitude and spectral characteristics), the translation controller must be insensitive to such disturbances.

Another critical area is the compatibility of the charge identification method with the realistic constraints of the translation controller and device/model errors. The charge identification scheme invokes the artificial acceleration of the proof mass in order to identify the charge disturbance. A major concern is that the identification accelerations are 3 to 5 orders of magnitude greater than the one we wish to measure.

Obviously, we cannot proceed to implement the identification filter without a comprehensive analysis of its impacts on the general drag-free design and its basic viability. This effort must include sensitivity to charge model errors, plate potential errors, the impact of integral control in reducing these errors, translation control stability constraints on identification frequencies and accelerations, and the feasibility of active charge removal during close encounter, i.e., intermittent proof mass grounding.

A methodology must be developed for the translation controller parameter(s) definition and selection. Techniques for bandwidth and gain setting with adaptability to a wide range of time-varying conditions during encounter must be found which provide autonomous control stability and optimum performance of the integral-error loops. This control technology must not rely on the assumption of well known error and disturbance models; it must instead employ predict/observe/correct logic to obtain in-situ high precision while protecting against out-of-limit conditions.

In the future as the Starprobe simulation programs continue to be used for both systems level and component level evaluation better models of the near solar environment, the spacecraft configuration, and the multi-experiment dynamic scenarios will be needed. More specific descriptions of these areas are necessary in order for control system requirements to be completely defined. With these specifications, the programs can be used to evaluate the proposed hardware and software adequacy. In this way these computer tools serve in every phase of the control system analysis, design, and verification. Expansion of the simulation programs to encompass all the interactive elements of the spacecraft will also be a parallel task as the aforementioned definition evolves.

REFERENCES

1. A. Vijayaraghavan, D. Sonnabend, T. Hagstrom, "Electrostatic Disturbance Forces on a 3-Axis Drag-Free Sensor," AIAA Paper 82-0046, AIAA 20th Aerospace Sciences Meeting, Jan. 11, 1982.

2. Hagstrom, T., "Drag-Free Proof Mass Electrostatic Force Model," JPL internal document EM 347-89, Sept. 9, 1980.

3. Jazwinski, A.H.,"Stochastic Processes and Filtering Theory," 1970, Academic Press.

4. "Drag-Free Estimation Feasibility Study," JPL Publication 80-20, May 15, 1980.

5. "Solar Probe Final Report of 1979 Study," JPL internal document 715-5, Dec. 14, 1979.

6. "STARPROBE Science Options Study and Final Report 1980-81, Advanced Technical Development Studies," JPL internal document 715-127, July 1981.

7. Harel, Moshe, et al., "Charging of the Proof Mass During the STARPROBE Mission," JPL internal document 5137-81-148, Nov. 3, 1981

8. Mettler, E., "Description of a Surface Force Control System for Planetary Probes," JPL internal document 344-493-EM, Dec. 26, 1974.

APPENDIX A

DISTURBANCE EFFECTS

A partial list of forces contributing to model errors includes solar pressure, control forces, kinematic effects due to the accelerated S/C fixed frame, moving masses, and self-gravity. Below we give a brief analysis of each of these forces and their relative impact on the charge identification problem.

The solar pressure is a slowly varying parameter, and its variation over 500 seconds is negligible. If a perfectly symmetrical S/C remained exactly nadir pointed, a very precise estimate of the acceleration resulting from the solar pressure might be attained. (This would be somewhat analogous to estimating the charge with 10^5 V.) What is not certain is the variation in this acceleration as a function of S/C attitude and non-symmetries. This is design dependent and merits further analysis.

Errors introduced by thruster mismodeling are, at worst, transient since these errors only occur while the thrusters are on. This source of error can be circumvented by not updating the charge estimate at these times.

Kinematic and moving mass effects are also design dependent, and it remains to determine whether these terms need to be incorporated into the charge estimator. We can however state with certainty that they present no problem. The reason for this follows.

The total disturbance created by these effects is

$$\ddot{\rho} + 2\omega \times (\dot{\rho}-\dot{r}) + \dot{\omega}x(\rho-r) + \omega x(\omega x(\rho-r)) \qquad (A\text{-}1)$$

Based on the torque and momentum storage available from the reaction wheels, upper bounds of 3×10^{-3} rad/sec and 3×10^{-5} rad/sec^2 can be

placed on ω and $\dot{\omega}$ respectively. We remark that these magnitudes can only be attained while the S/C is executing an imaging slew and in general would be an order of magnitude less. Now $\ddot{\rho}$ appears as a result of a reaction force from translating or rotating a mass (antenna, platform, etc.) Such forces would not exceed a few thousandths of a newton; and from the drag-free control law we obtain a bound of 1.5 mm/sec on $|\dot{\mathbf{r}}|$. Putting these considerations together and allowing for a 10 cm offset in the center of mass, as a worst case (A-1) is in the $10\mu/sec^2$ range. In such an event incorporation of these terms would become necessary. This is the magnitude of the unmodeled disturbance used in the charge estimation simulations.

For estimation purposes the pertinent question is how good is our knowledge of these disturbances? In Appendix B it is shown that even in the worst case these accelerations can be modeled to within $.5\mu/sec^2$.

Self-gravity accelerations are in the $10^{-2}\mu/sec^2$ range and therefore have negligible impact on the charge estimation problem.

Strong Electrostatic Charging

We have already noted the impact of increasing charge levels on the identification problem. A recent study [7] has shown a remote but finite possibility that the charge on the proof mass may exceed 10^{-10} coulombs in the solar encounter. It behooves us to indicate the severity of the problems associated with much greater magnitudes and suggest possible solutions. These extreme levels apply to the case of an "extraordinary" solar flare incident, and the Jovian environment in general.

To illustrate the control problem due to very strong charge we take the value $q = 10^{-7}$ coulomb; then from (4.11) the acceleration due to

this charge is calculated to be

$$\frac{q^2N}{\epsilon_o mb^3R}\,|r_z| \approx 68 \times |r_z|/\text{sec}^2 \ .$$

Therefore if the proof mass is displaced 1.0 mm from the cavity center, the acceleration above is 680 times that of maximum solar pressure during sun encounter. Consequently there would not be sufficient translation control authority to return the proof mass to the cavity center. However, there are some parameters that can be adjusted to diminish the charge effect. For example, increasing the mass (m) of the proof mass will linearly decrease the charge acceleration, and an increase in the cavity radius b (with a proportional increase in the proof mass radius) will result in a cubic decrease of the acceleration. Thus modifying the proof mass-cavity configuration is a possible method for restoring the robustness of the controller.* Another approach would be to narrow the deadband. But this offers only linear improvement and results in a higher bandwidth controller.

For the sake of argument, let us assume that the control problem has been overcome by some combination of the remedies offered above. We still must confront the charge problem. Suppose both the cavity radius and the proof sphere's mass were increased an order of magnitude. This would yield a decrease in the charge acceleration of 4 orders of magnitude. Even with this new geometry, a submicron displacement of the proof mass would result in an acceleration greater than the drag-free objective of 10^{-9} m/sec^2. It is evident then that any controller approach to reduce charge effects is inadequate, and a charge identification is still necessary.

Staying with this new configuration, the error criterion (4.12) becomes

$$|q - \hat{q}| < \frac{1.5 \times 10^{-21}}{|r_z||q + \hat{q}|}$$

*We have not considered how geometry modifications impact sensor resolution.

A proof mass displacement of 1.0 mm would then require better than 1 part in 10^4 accuracy in the charge estimate to guarantee a 10^{-9}m/sec^2 error in the estimated acceleration. This is certainly far better than the 1 part in 10^8 required by the old geometry, but it is still unacceptably severe. In any case geometry "fiddling" is at least suggestive of directions to pursue in this problem.

Although the strong charge problem is indeed formidable, it would be premature to conclude that its associated difficulties are insurmountable. We are merely pointing out that while the software methods (estimation, integral control) developed in this report are effective in compensating/reducing disturbances 1 or 2 orders of magnitude, a more design integrated strategy is necessary for this extreme problem. This would include investigation of various sensor geometries, greater shielding of the cavity, discharging of the proof mass, ultra-high resolution displacement sensing, etc., to bring the charge into the range where integral control and the error compensation model approach are viable.

APPENDIX B

PROOF MASS STATE ESTIMATOR DESIGN

Without further analysis into the charge identification scheme's impact on the drag free mission, we feel that it is appropriate at this time to consider the charge as an intermittently estimated state. With this in mind we construct two estimators.

The sole purpose of the first estimator is to provide knowledge of the proof mass position and velocity. As was demonstrated in the simulations of Section III, there is negligible gain in including angular rate and acceleration information in this filter design. Therefore we may ignore these terms and decouple the estimator (3.2). The resulting steady state filter for the z-axis is

$$\frac{d}{dt}\begin{bmatrix}\hat{r}_z\\ \dot{\hat{r}}_z\end{bmatrix} = \begin{bmatrix}0 & 1\\ 0 & 0\end{bmatrix}\begin{bmatrix}\hat{r}_z\\ \dot{\hat{r}}_z\end{bmatrix} + \begin{bmatrix}0\\ u(t) + a_{sp}\end{bmatrix} + \begin{bmatrix}k_1\\ k_2\end{bmatrix}(y-\hat{r}_z) \qquad (B.1)$$

with $k_1 = 2$, $k_2 = 2$. The filters for the other axes are obtained by substitution of the appropriate subscripts in (B.1).

In contrast with the filter above, the analysis in Appendix A suggests the need for retaining the angular rate, angular acceleration, and center of mass position/motion information in the charge estimator design. It is conceivable to incorporate these terms into the state of the charge estimator, but a reasonable consideration for on-board implementation of the filter is to avoid introducing additional states when possible. Thus we shall consider them as previously estimated inputs to the estimator. The filter equations (4.9) then become

$$
\begin{aligned}
\dot{\hat{x}}_1 &= \hat{x}_2 + \frac{P_{11}}{r}(y - \hat{x}_1) \\
\dot{\hat{x}}_2 &= \frac{2V(t)\hat{q}\,PA}{mbR} + \frac{\varepsilon_o}{mb}\left[V^2(t)\left(2L - \frac{4p^2A^2}{R}\right) + \frac{\hat{q}^2N}{\varepsilon_o^2 b^2 R}\right]\hat{x}_1 + u(t) + \\
&\quad a_{sp} + \ddot{\hat{\rho}}_z + 2\{\hat{\omega}_x(\dot{\hat{\rho}}_y - \dot{\hat{r}}_y) - \hat{\omega}_y(\dot{\hat{\rho}}_x - \dot{\hat{r}}_x)\} + \dot{\hat{\omega}}_x(\hat{\rho}_y - \hat{r}_y) \qquad \text{(B.3)} \\
&\quad - \dot{\hat{\omega}}_y(\hat{\rho}_x - \hat{r}_x) + \hat{\omega}_x\{\hat{\omega}_z(\hat{\rho}_x - \hat{r}_x) - \hat{\omega}_x(\hat{\rho}_z - \hat{r}_z)\} - \\
&\quad \hat{\omega}_y\{\hat{\omega}_y(\hat{\rho}_z - \hat{r}_z) - \hat{\omega}_z(\hat{\rho}_y - \hat{r}_y)\} + \frac{P_{21}}{r}(y - \hat{x}_1) \\
\dot{\hat{q}} &= \frac{P_{31}}{r}(y - \hat{x}_1)
\end{aligned}
$$

and $P = (P_{ij})$ satisfies (4.9b).

In the interest of maintaining the decoupled nature of the filter, in the equations above we take $\hat{r}$ and $\dot{\hat{r}}$ to be estimates supplied by the <u>first</u> filter. The alternative to this would be to incorporate these terms into a filter based on the original dynamics (4.1). But then a 7 x 7 covariance equation would result instead of the 3 x 3 as in (4.9b). Therefore this slight alteration eliminates the need for solving 22 coupled differential equations!

We remark that these filter equations represent a worst case in that it may not be necessary to include all the dynamic and kinematic terms. For example, taking an objective of modeling these disturbances to within $.1\mu/sec^2$, the second order angular rate terms would not have to be modeled if the center of mass remained within 1 cm of the cavity center. In any event, we proceed to develop estimates of these terms below.

We first consider estimating ω_x and $\dot{\omega}_x$ (the extension to the other axes will be obvious). Let I_{xx}, I_{yy}, and I_{zz}, denote the S/C's moments of inertia, and let T_x denote the component of the torque vector along the x-axis. Assuming $|(I_{yy} - I_{zz})|\omega_y\omega_z| << T_x$ and small products of inertia, the situation is characterized by the dynamics

$$\dot{\omega}_x = T_{xx}/I_{xx} \tag{B.4}$$

and the observations

$$y_{t_i} = \Delta\theta_{t_i} + \varepsilon_{t_i} \tag{B.5}$$

where y_{t_i} is the gyro output - an incremental position vector, $\Delta\theta_{t_i} \approx \omega_x(t_i)\Delta t$, $\Delta t = (t_i - t_{i-1})$, and ε_{t_i} is an error.

For $|\dot{\omega}| < 5 \times 10^{-6}$ rad/sec^2 and $|\rho| < 1$ cm, the contribution of the term $[\dot{\omega}x(\rho-r)]_z$ to the total disturbance is less than .05μ/sec^2. Assuming the attitude control authority is an order of magnitude greater than the disturbance torques, the assumption on $|T_x|$ is valid when $\dot{\omega}_x$ warrants consideration in the filter design. Thus by defining $\dot{\omega}_x = \hat{T}_x/\hat{I}_{xx}$, where $\hat{T}_x$ is the feed forward control torque and $\hat{I}_{xx}$ is an estimate of I_{xx} obtained by say calibration, the estimate error here is

$$|\dot{\omega}_x - \hat{\dot{\omega}}_x| \leq |\hat{T}_x/\hat{I}_{xx} - T_x/I_{xx}|$$

$$\leq \hat{T}_x/I_{xx}\hat{I}_{xx}\,|I_{xx} - \hat{I}_{xx}| + \frac{1}{I_{xx}}\,|T_x - \hat{T}_x|$$

Then 10% errors in the estimates of T_x and I_{xx} would then yield about a 20% error in the estimate of $\dot{\omega}_x$. Using $|\dot{\omega}|_{max} < 3 \times 10^{-5}$ rad/sec^2, we obtain $|\dot{\omega}_x - \hat{\dot{\omega}}_x| < 6 \times 10^{-6}$ rad/sec^2.

The easiest approach for obtaining ω_x is to form the quotient $y_{t_i}/\Delta t$. The error incurred here is

$$|\omega_x(t_i) - \omega_x(t_i)| \leq |\varepsilon_{t_i}/\Delta t| + |\Delta\theta_{t_i}/\Delta t - \omega_x(t_i)|$$

$$\leq |\varepsilon_{t_i}/\Delta t| + \max_{t\in[t_{i-1},t_i]} |\omega_x(t) - \omega_x(t_i)|$$

$$\leq |\varepsilon_{t_i}|/\Delta t + \Delta t\,|\dot{\omega}_x(t)|_{max}$$

Taking $\Delta t = .01$ sec, $|\dot{\omega}_x|_{max} < 3 \times 10^{-5}$ rad/sec^2, and $|\varepsilon_t| < 10^{-7}$ rad ($\approx .02$ arc sec), the error above is then bounded by 10^{-5} rad/sec.

Now we turn to the question of estimating the center of mass and its derivatives in the presence of moving masses. The focus here is on moving platforms and appendages rather than the "slow" effects of fuel depletion and thermal distortion.

To obtain these estimates we decompose the S/C into two components.

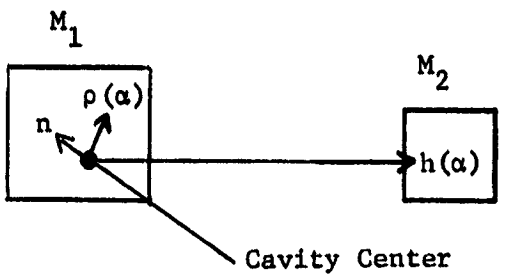

Here M_2 represents a moving mass (m_2 = its mass), M_1 represents the remainder of the S/C (m_1 = its mass), $h(\alpha)$ the center of mass of M_2 (α is a measured parameter from which $h(\alpha)$ is known), n the center of mass of M_1, and $\rho(\alpha)$ the center of mass of the S/C. Then clearly

$$\rho(\alpha) = \frac{m_1}{m_1 + m_2}\, n + \frac{m_2}{m_1 + m_2}\, h(\alpha) \qquad (B.6)$$

From (B.6) we obtain the derivatives with respect to the S/C frame;

$$\dot{\rho} = \frac{m_1}{m_1 + m_2}\, h'(\alpha)\dot{\alpha}, \quad \ddot{\rho} = \frac{m_2}{m_1 + m_2}\, [h'(\alpha)\ddot{\alpha} + h''(\alpha)\dot{\alpha}^2] \ .$$

Since $h(\alpha)$ is known from the geometry and measurement of α, it remains to determine $\dot{\alpha}$ and $\ddot{\alpha}$. But these are readily obtained from the force acting on M_2. Let F_α denote this force. Then,

$$\frac{d^2}{dt^2}\,(\rho(\alpha) - h(\alpha)) = F_\alpha/m_2 \qquad (B.7)$$

Now recalling (B.6)

$$\frac{d^2}{dt^2}\,(h(\alpha) - n) = \frac{m_1 + m_2}{m_1\, m_2}\; F_\alpha \qquad (B.8)$$

And in S/C coordinates (B.8) becomes

$$\ddot{\alpha}h'(\alpha)+\dot{\alpha}^2h''(\alpha)+2\dot{\alpha}\omega xh'(\alpha)+\dot{\omega}x(h(\alpha)-n)+\omega x(\omega x(h(\alpha)-n)) = \frac{m_1 + m_2}{m_1\, m_2}\, F_\alpha \qquad (B.9)$$

This equation is not as bad as it looks. For example, if $h(\alpha)$ represents a translation, say $h(\alpha) = \alpha z$, z = unit vector, α = displacement, then $h''(\alpha) = 0$. Furthermore, under our present assumptions on $|\omega|$ $|\dot{\omega}|$ etc., (B.9) effectively reduces to

$$\ddot{\alpha} = \frac{m_1 + m_2}{m_1\, m_2}\; |F_\alpha|$$

And from this it follows that

$$\ddot{\rho} = \frac{F_\alpha}{m_1}$$

As precise knowledge of both the actuator force F_α and the mass of the moving appendage or platform is expected, the error in the estimates of $\dot{\rho}$ and $\ddot{\rho}$ will be driven by the error in the S/C mass estimate.

In any case, with the estimation schemes outlined above, the total model error contribution of the kinematic and moving mass effects can probably be kept below $.5\mu/sec^2$.

APPENDIX C

```
PROGRAM  STAR PROBE SPACECRAFT SIMULATION                                    ...
         THREE AXES STABILIZED RIGID BODY CONTROL                            ...
         1981 CONICAL SHAPE CONFIGURATION                                    ...
         FULL SCIENCE OPTION WITH 30 DEG HEAT SHIELD                         ...
         RETRACTED HIGH GAIN ANTENNA                                         ...
         CONDITIONS AT PERIHELION

 COMMENT CREATED 01 MAY 1981 BY R.W. KEY                                     ...
         METRIC UNITS THROUGHOUT (N-M-S)                                     ...
         MASS PROPERTIES FROM D. NOON (JUN 81)                               ...
         DRAG FREE ESTIMATOR DESIGN BY M. MILMAN (MAY 81)                    ...
         DRAG FREE CONTROLLER DESIGN BY D. SCHAECHTER (OCT 80)               ...
         HYDRAZINE GAS JET CONTROLLER DESIGN BY P. MAC (JULY 80)

 INTEGER J,K,MANNBR,JJ,JP1,JP8,JP9
   ARRAY SCCMLV(3)     , GJCLV(4,3)    , GJFV(16,3)    , SCINRT(6)     ,...
         FSC(3)        , TSC(3)        , CMTCPV(3)     , PMCCLV(3)     ,...
         CMTGJV(4,3)   , CPLV(3)       , JETON(16)     , FGJC(4,3)     ,...
         FGJ(3)        , TGJC(4,3)

 DROP

  COMMENT ************************************************************
  COMMENT ********************* S/C MASS PROPERTIES **********************
  COMMENT ************************************************************

     DATA SCINRT/4750.0,4700.0,1700.0,0.0,0.0,0.0/

  COMMENT ******** S/C CM LOCATION VECTOR IN CAVITY COORDINATES *********

     DATA SCCMLV /+0.00,+0.00,+0.00/

  COMMENT ************************************************************
  COMMENT ****** LOCATION OF GAS JET CLUSTERS IN CAVITY COORDINATES *****
  COMMENT ************************************************************

     DATA (GJCLV(1,J),J=1,3) /+2.0, 0.0,+0.0/
     DATA (GJCLV(2,J),J=1,3) / 0.0,+2.0,+0.0/
     DATA (GJCLV(3,J),J=1,3) /-2.0, 0.0,+0.0/
     DATA (GJCLV(4,J),J=1,3) / 0.0,-2.0,+0.0/

  COMMENT ********** VECTORS FROM S/C CM TO GAS JET CLUSTERS ************

          DO L1 K=1,4
          DO L1 J=1,3
          CMTGJV(K,J)=GJCLV(K,J)-SCCMLV(J)
     L1.. CONTINUE

  COMMENT ************************************************************
          NXQINT=0.

  PICKUP

  INITIAL
  CONSTANT PIE=3.14159265       ,       G=9.80665
```

```
COMMENT ********************************************************
        *                                                      *
        *       DEFINE THE S/C FIXED AXES AS FOLLOWS:          *
        *       ------------------------------------           *
        *                                                      *
        *       X = HGA DEPLOYMENT DIRECTION                   *
        *                                                      *
        *       Y = DEXTRAL COMPLEMENT                         *
        *                                                      *
        *       Z = HEAT SHIELD AXIS OF SYMMETRY               *
        *                                                      *
        *       ORIGIN IS CENTER OF PROOF MASS CAVITY          *
        *                                                      *
        ********************************************************



        ********************************************************
        *                                                      *
        *       SELECT THE MANEUVER BY ITS NUMBER              *
        *       ---------------------------------              *
        *                                                      *
        *       1 - TURN ENTIRE SPACECRAFT ABOUT X AXIS        *
        *                                                      *
        *       2 - TURN ENTIRE SPACECRAFT ABOUT Y AXIS        *
        *                                                      *
        *       3 - TURN ENTIRE SPACECRAFT ABOUT Z AXIS        *
        *                                                      *
        *       4 - ACQUISITION OF INERTIAL REFERENCES         *
        *                                                      *
        *       5 - SOLAR FLYBY (PERIHELION)                   *
        *                                                      *
        ********************************************************
        *                                                      *
        *                                                      *
CONSTANT                    MANEUV = 5.0
 COMMENT *                                                    *
        *                                                      *
        ********************************************************



        ********************************************************
        *                                                      *
        *       DRAG FREE TRAJECTORY INFORMATION               *
        *       --------------------------------               *
        *                                                      *
        *                                                      *
        *    HELIOCENTRIC COORDINATE REFERENCE FRAME           *
        *       1 AU = 1.4960E+11 (M)                          *
        *       SOLAR RADIUS = 0.0046524 (AU)                  *
        *                                                      *
        *    PERIHELION ALTITUDE (AU)                          *
        *
CONSTANT        PERALT = 0.01861
        *                                                      *
        ********************************************************
```

```
*****************************************************************
*                                                               *
*       SET PROOF MASS INITIAL CONDITIONS                       *
*       ---------------------------------                       *
*                                                               *
*       X AXIS              Y AXIS              Z AXIS          *
*       ------              ------              ------          *
*                                                               *
COMMENT *                                                       *
*    PROOF MASS INITIAL VELOCITY (M/SEC)                        *
*                                                               *
CONSTANT        PMXDI=0.0    ,     PMYDI=0.0    ,     PMZDI=0.0
 COMMENT *                                                      *
*    PROOF MASS INITIAL TRAJECTORY POSITION (M)                 *
*                                                               *
CONSTANT        PMXI=0.0     ,     PMYI=0.0     ,     PMZI=0.0
 COMMENT *                                                      *
*                                                               *
*****************************************************************


*****************************************************************
*                                                               *
*       SET SPACECRAFT INITIAL CONDITIONS                       *
*       ---------------------------------                       *
*                                                               *
*       X AXIS              Y AXIS              Z AXIS          *
*       ------              ------              ------          *
*                                                               *
*    INITIAL ANGULAR RATES (RAD/SEC)                            *
*                                                               *
CONSTANT        WXI=0.0        , WYI=1.11E-4      ,    WZI=0.0
 COMMENT *                                                      *
*    INITIAL ANGULAR POSITION (RAD)                             *
*                                                               *
CONSTANT        THETXI=0.0     ,  THETYI=0.0      ,  THETZI=0.0
 COMMENT *                                                      *
*    INITIAL TRANSLATIONAL RATES  (M/SEC)                       *
*                                                               *
CONSTANT        SCXDI=0.0      ,  SCYDI=0.0       ,  SCZDI=0.0
 COMMENT *                                                      *
*    INITIAL TRANSLATIONAL POSITION (M)                         *
*                                                               *
CONSTANT        SCXI=0.00      ,  SCYI=0.00       ,  SCZI=+0.00025
 COMMENT *                                                      *
*                                                               *
*****************************************************************
```

```
*****************************************************************
*                                                               *
*       TURN COMMAND INFORMATION                                *
*       ------------------------                                *
*                                                               *
*    NADIR POINTING TURN RATE COMMANDS                          *
*                                                               *
CONSTANT      NADIRX=0.0       , NADIRY=1.11E-4  , NADIRZ=0.0
 COMMENT *                                                      *
*                                                               *
*    COMMANDED SPACECRAFT TURN RATES (RAD/SEC)                  *
*                                                               *
CONSTANT                TRNTIM = 0.00
CONSTANT      TRNXRT=1.745E-3, TRNYRT=1.745E-3, TRNZRT=1.745E-3
 COMMENT *                                                      *
*                                                               *
*****************************************************************

*****************************************************************
*                                                               *
*       CONTROL SYSTEM ON/OFF SWITCHS                           *
*       -----------------------------                           *
*                                                               *
CONSTANT       TCSON=1.0              ,          ACSON=1.0
 COMMENT *     ---------              ,          --------        *
*     DRAG FREE              GAS JETS        REACTION WHEELS    *
*                                                               *
CONSTANT       DFON=1.0       ,       GJON=0.0     ,      RWON =1.0
 COMMENT *                                                      *
*                                                               *
*****************************************************************

*****************************************************************
*                                                               *
*       SET SIMULATION TIME                                     *
*       -------------------                                     *
*                                                               *
CONSTANT            FINTIM = 9.999     ,       SIMTIM = 5.00
 COMMENT *                                                      *
*                                                               *
*****************************************************************

      TRNXON=0.0 $ TRNYON=0.0 $ TRNZON=0.0
      MANNBR=MANEUV+.5     $     GO TO (M1,M2,M3,M4,M5), MANNBR
M1..  TRNXON=1.0    $    GO TO MEND
M2..  TRNYON=1.0    $    GO TO MEND
M3..  TRNZON=1.0    $    GO TO MEND
M4..  TCSON =0.0    $    GO TO MEND
M5..  CONTINUE
MEND..CONTINUE
```

```
COMMENT ************************************************************
COMMENT ***************** REACTION WHEEL PARAMETERS ******************
COMMENT ************************************************************

        TRWMAX=1.00   $ COMMENT MAXIMUM REACTION WHEEL TORQUE CAPABILITY

COMMENT ************************************************************
COMMENT ***************** GAS JET THRUSTER PARAMETERS ****************
COMMENT ************************************************************

CONSTANT GASUSE=0.0                $   COMMENT INITILIZE GAS USED
CONSTANT GJMOT = 0.010             $   COMMENT GAS JET MINIMUM ON TIME
CONSTANT ISP = 115.0               $   COMMENT SPECIFIC IMPULSE OF N2H4
CONSTANT F1JET=0.4448              $   COMMENT FORCE OF ONE JET = 0.1 LB
         CANT=62.0*PIE/180.0       $   COMMENT CANT ANGLE OF JETS 9 THRU 16
         FCJS=F1JET*SIN(CANT)      $   COMMENT FORCE OF A CANTED JET
         FCJC=F1JET*COS(CANT)      $   COMMENT CANT ANGLE W.R.T. XY PLANE
         GMFLOW=F1JET/(ISP*G)

COMMENT ************** DEFINE EACH GAS JET FORCE VECTOR **************

         GJFV(1,1)=0.0      $  GJFV(1,2)=0.0      $  GJFV(1,3)=+F1JET
         GJFV(2,1)=0.0      $  GJFV(2,2)=0.0      $  GJFV(2,3)=+F1JET
         GJFV(3,1)=0.0      $  GJFV(3,2)=0.0      $  GJFV(3,3)=+F1JET
         GJFV(4,1)=0.0      $  GJFV(4,2)=0.0      $  GJFV(4,3)=+F1JET
         GJFV(5,1)=0.0      $  GJFV(5,2)=0.0      $  GJFV(5,3)=+F1JET
         GJFV(6,1)=0.0      $  GJFV(6,2)=0.0      $  GJFV(6,3)=+F1JET
         GJFV(7,1)=0.0      $  GJFV(7,2)=0.0      $  GJFV(7,3)=+F1JET
         GJFV(8,1)=0.0      $  GJFV(8,2)=0.0      $  GJFV(8,3)=+F1JET
         GJFV(9,1)=0.0      $  GJFV(9,2)=+FCJC    $  GJFV(9,3)= -FCJS
         GJFV(10,1)=0.0     $  GJFV(10,2)=-FCJC   $  GJFV(10,3)=-FCJS
         GJFV(11,1)=-FCJC   $  GJFV(11,2)=0.0     $  GJFV(11,3)=-FCJS
         GJFV(12,1)=+FCJC   $  GJFV(12,2)=0.0     $  GJFV(12,3)=-FCJS
         GJFV(13,1)=0.0     $  GJFV(13,2)=-FCJC   $  GJFV(13,3)=-FCJS
         GJFV(14,1)=0.0     $  GJFV(14,2)=+FCJC   $  GJFV(14,3)=-FCJS
         GJFV(15,1)=+FCJC   $  GJFV(15,2)=0.0     $  GJFV(15,3)=-FCJS
         GJFV(16,1)=-FCJC   $  GJFV(16,2)=0.0     $  GJFV(16,3)=-FCJS

COMMENT ************************************************************
COMMENT ************** ON BOARD COMPUTER PARAMETERS ******************
COMMENT ************************************************************

COMMENT SET EXECUTION INTERVAL FOR ATTITUDE CONTROL ALGORITHMS
        ACSINC=CI

COMMENT SET EXECUTION INTERVAL FOR TRANSLATION CONTROL ALGORITHMS
        TCSINC=CI

COMMENT INITIALIZE S/C TURN COMMAND INFORMATION

        TURNON=1.0
        TRINCX=TRNXRT*ACSINC*TRNXON    $   NADIRX=NADIRX*ACSINC
        TRINCY=TRNYRT*ACSINC*TRNYON    $   NADIRY=NADIRY*ACSINC
        TRINCZ=TRNZRT*ACSINC*TRNZON    $   NADIRZ=NADIRZ*ACSINC
        TRNCOX=0.0     $   TRNCOY=1.00455E-3     $   TRNCOZ=0.0
```

```
 COMMENT ******** ATTITUDE RATE+POSITION CONTROLLER PARAMETERS *********

 COMMENT REACTION WHEEL CONTROL LOOP PARAMETER VALUES

CONSTANT RWKPTX = 114.4      ,   RWKPTY = 114.6        ,   RWKPTZ = 114.6
CONSTANT RWKRPX = 9.10       ,   RWKRPY =  9.06        ,   RWKRPZ = 5.45

 COMMENT GAS JET CONTROL LOOP PARAMETER VALUES

         ACSDB=0.050*PIE/180.0   $   COMMENT GAS JET ACS DEAD BAND SIZE
CONSTANT GJKRPX = 4.75       ,   GJKRPY = 4.70         ,   GJKRPZ = 1.7

 COMMENT ATTITUDE RATE ESTIMATOR PARAMETER VALUES

 COMMENT ATESKX = 0.0        ,   ATESKY = 0.0          ,   ATESKZ = 0.0


 COMMENT ************ TRANSLATION CONTROLLER PARAMETERS ***************

CONSTANT SCMASS=1000.0
CONSTANT TCSDB=0.005         $   COMMENT  TCS DEAD BAND SIZE
CONSTANT ZDBOFF=-0.00442     $   COMMENT  Z DEAD BAND SWITCH OFF LINE
CONSTANT DFKRPX = 0.5        ,   DFKRPY =  0.5         ,   DFKRPZ = 0.5
CONSTANT DFINKX = 0.0        ,   DFINKY =  0.0         ,   DFINKZ = 0.0
         INTERX = 0.0        $   INTERY =  0.0         $   INTERZ = 0.0

 COMMENT INITIALIZE POSITION INFOMATION FOR OBC

         SCXPMI=SCXI-PMXI    $   SCYPMI=SCYI-PMYI      $   SCZPMI=SCZI-PMZI
         SCXESI=SCXPMI       $   SCYESI=SCYPMI         $   SCZESI=SCZPMI
         SCXDPI=SCXDI-PMXDI  $   SCYDPI=SCYDI-PMYDI    $ SCZDPI=SCZDI-PMZDI
         SCXDEI=SCXDPI       $   SCYDEI=SCYDPI         $   SCZDEI=SCZDPI

 COMMENT ESTIMATOR KNOWLEDGE OF THE S/C CM

         SCCMXE=SCCMLV(1)    $   SCCMYE=SCCMLV(2)      $   SCCMZE=SCCMLV(3)

 COMMENT DRAG FREE ESTIMATOR PARAMETER VALUES

CONSTANT R=0.04
CONSTANT P11I=1.E+2          ,     P22I=3.E+2          ,     P33I=1.E+2
CONSTANT P44I=3.E+2          ,     P55I=1.E+2          ,     P66I=3.E+2
CONSTANT SGPX=10.E+2         ,     SGPY=10.E+2         ,     SGPZ=10.E+2
         ERX=0.0             $     ERY=0.0             $     ERZ=0.0
         ERXD=0.0            $     ERYD=0.0            $     ERZD=0.0

 COMMENT ************************************************************
 COMMENT ***************** DISTURBANCE MODEL DATA ********************
 COMMENT ************************************************************
CONSTANT DISTON = 1.0        $     COMMENT ON/OFF SWITCH FOR DISTURBANCES

         TDISTX=0.00         $     TDISTY=0.00          $     TDISTZ=0.00
         FDISTX=0.00         $     FDISTY=0.00          $     FDISTZ=0.00
```

```
 COMMENT ****************** SOLAR RADIATION MODEL ***********************

 COMMENT SOLAR RADIATION FORCE EQUIVELENT TO 10E-5 "G"

         FSR=SCMASS*G*1.E-5     $   COMMENT RANDOM FSR MEAN VALUE
         FSRSIG=FSR/10.0        $   COMMENT RANDOM FSR STANDARD DEVIATION
         FSRCTC=10.0            $   COMMENT RANDOM FSR CORRELATION TIME

 COMMENT ******** PROOF MASS CHARGE IDENTIFICATION DISTURBANCE *********

CONSTANT PMMASS=0.20            $   COMMENT  PM MASS (KG)
CONSTANT IDVOLT=1000.0          $   COMMENT  PM CHARGE ID VOLTAGE
CONSTANT IDK2=2.4E-8            $   COMMENT  PM CHARGE ID CONSTANT

 COMMENT ************************************************************

         PZI,P1I,P2I,P3I=HCK(INITL,THETXI,THETYI,THETZI)
         NXQDYN=0.   $   NXQDER=0.   $   NXQTER=0.   $   NXQINT=NXQINT+1.
END
DYNAMIC
         VARIABLE T=0.00  $  TIME=T-SIMTIM  $  IF(T.GT.FINTIM)GO TO FIN
         DEBUG T,1,0.
         DERPDY=NXQDER-NXDERL  $  NXDERL=NXQDER  $  NXQDYN=NXQDYN+1.

         THETAX=2.0*P1    $    THETAY=2.0*P2    $    THETAZ=2.0*P3

 COMMENT ************************************************************
 COMMENT *************** OUTPUT AND PLOTTING INFORMATION **************
 COMMENT ************************************************************

         OUTPUT 100,  TIME   ,   TIME   ,   TIME   ,   ...
                      THETAX,   THETAY,   THETAZ,   ...
                      TRNCOX,   TRNCOY,   TRNCOZ,   ...
                      WX    ,   WY    ,   WZ    ,   ...
                      WXEST ,   WYEST ,   WZEST ,   ...
                      WXD   ,   WYD   ,   WZD   ,   ...
                      COERRX,   COERRY,   COERRZ,   ...
                      XCONON,   YCONON,   ZCONON,   ...
                      TDESRX,   TDESRY,   TDESRZ,   ...
                      TRWX  ,   TRWY  ,   TRWZ  ,   ...
                      TSCX  ,   TSCY  ,   TSCZ  ,   ...
                      FGJX  ,   FGJY  ,   FGJZ  ,   ...
                      FSCX  ,   FSCY  ,   FSCZ  ,   ...
                      PMX   ,   PMY   ,   PMZ   ,   ...
                      PMXD  ,   PMYD  ,   PMZD  ,   ...
                      PMXDD ,   PMYDD ,   PMZDD ,   ...
                      SCX   ,   SCY   ,   SCZ   ,   ...
                      SCXD  ,   SCYD  ,   SCZD  ,   ...
                      SCXDD ,   SCYDD ,   SCZDD ,   ...
                      SCXPM ,   SCYPM ,   SCZPM ,   ...
                      SCXOB ,   SCYOB ,   SCZOB ,   ...
                      SCXEST,   SCYEST,   SCZEST,   ...
                      SCXDPM,   SCYDPM,   SCZDPM,   ...
                      SCXDES,   SCYDES,   SCZDES,   ...
                      XHDD  ,   YHDD  ,   ZHDD  ,   ...
                      SCXAPM,   SCYAPM,   SCZAPM,   ...
```

```
                DFERRX,   DFERRY,   DFERRZ,   ...
                DFXCON,   DFYCON,   DFZCON,   ...
                INTERX,   INTERY,   INTERZ,   ...
                RANDOM,   NJETON,   GASUSE,   ...
                TDISTX,   TDISTY,   FDISTZ,   ...
                NXQDER,   NXQDYN,   DERPDY
PREPAR   11           ,   DERPDY,   TIME  ,   ...
                THETAX,   THETAY,   THETAZ,   ...
                WX    ,   WY    ,   WZ    ,   ...
                TSCX  ,   TSCY  ,   TSCZ  ,   ...
                FSCX  ,   FSCY  ,   FSCZ  ,   ...
                ABERX ,   ABERY ,   ABERZ ,   ...
                ABERXD,   ABERYD,   ABERZD,   ...
                PMZ   ,   PMZD  ,   SCZEST,   ...
                SCZ   ,   SCZD  ,   SCZDES,   ...
                SCXPM ,   SCYPM ,   SCZPM ,   ...
                SCXDPM,   SCYDPM,   SCZDPM,   ...
                INTERX,   INTERY,   INTERZ,   ...
                TRNCOY,   GASUSE
RANGE    ...
                THETAX,   THETAY,   THETAZ,   ...
                TRNCOX,   TRNCOY,   TRNCOZ,   ...
                WX    ,   WY    ,   WZ    ,   ...
                WXEST ,   WYEST ,   WZEST ,   ...
                WXD   ,   WYD   ,   WZD   ,   ...
                COERRX,   COERRY,   COERRZ,   ...
                XCONON,   YCONON,   ZCONON,   ...
                TDESRX,   TDESRY,   TDESRZ,   ...
                TRWX  ,   TRWY  ,   TRWZ  ,   ...
                TSCX  ,   TSCY  ,   TSCZ  ,   ...
                FGJX  ,   FGJY  ,   FGJZ  ,   ...
                FSCX  ,   FSCY  ,   FSCZ  ,   ...
                SCX   ,   SCY   ,   SCZ   ,   ...
                SCXD  ,   SCYD  ,   SCZD  ,   ...
                SCXDD ,   SCYDD ,   SCZDD ,   ...
                SCXPM ,   SCYPM ,   SCZPM ,   ...
                SCXEST,   SCYEST,   SCZEST,   ...
                PMX   ,   PMY   ,   PMZ   ,   ...
                PMXD  ,   PMYD  ,   PMZD  ,   ...
                PMXDD ,   PMYDD ,   PMZDD ,   ...
                ABERX ,   ABERY ,   ABERZ ,   ...
                ABERXD,   ABERYD,   ABERZD,   ...
                SCXDPM,   SCYDPM,   SCZDPM,   ...
                SCXDES,   SCYDES,   SCZDES,   ...
                SCXAPM,   SCYAPM,   SCZAPM,   ...
                DFERRX,   DFERRY,   DFERRZ,   ...
                DFXCON,   DFYCON,   DFZCON,   ...
                INTERZ,   NJETON,   GASUSE,   ...
                TDISTX,   TDISTY,   FDISTZ,   ...
                NXQDER,   NXQDYN,   DERPDY
```

```
COMMENT ************************************************************
COMMENT ********************** DRIRU II MODEL ************************
COMMENT ************************************************************
        IF (WX.GT.0.034907) WRITE (6,SAT)
        IF (WY.GT.0.034907) WRITE (6,SAT)
        IF (WZ.GT.0.034907) WRITE (6,SAT)
  SAT.. FORMAT (1X,'++++++++++++ GYRO SATURATION ++++++++++++')

COMMENT ************************************************************
COMMENT ********************** TCS SENSOR MODEL ***********************
COMMENT ************************************************************
        XNOISE=GAUSS(0.0,50.0E-6)     $     SCXOB=SCXPM+XNOISE
        YNOISE=GAUSS(0.0,50.0E-6)     $     SCYOB=SCYPM+YNOISE
        ZNOISE=GAUSS(0.0,50.0E-6)     $     SCZOB=SCZPM+ZNOISE

COMMENT ************************************************************
COMMENT ***************** ON BOARD COMPUTER PROCESSING ***************
COMMENT ************************************************************

        DO INITJ J=1,16    $     JETON(J)=0.0    $     INITJ.. CONTINUE

COMMENT ************** GENERATE S/C TURN COMMAND INPUTS **************

        IF (T.GE.TRNTIM) TURNON=0.0
        TRNCOX=TRNCOX+TRINCX*TURNON+NADIRX
        TRNCOY=TRNCOY+TRINCY*TURNON+NADIRY
        TRNCOZ=TRNCOZ+TRINCZ*TURNON+NADIRZ


COMMENT ******************* ATTITUDE RATE ESTIMATOR **********************

COMMENT ASSUME PERFECT ATTITUDE RATE ESTIMATION

        WXEST=WX      $      WYEST=WY      $      WZEST=WZ

COMMENT ************ GAS JET RATE+POSITION ATTITUDE CONTROL ************


COMMENT COERRX=(TRNCOX-THETAX-GJKRPX*WXEST)*ACSON
COMMENT COERRY=(TRNCOY-THETAY-GJKRPY*WYEST)*ACSON
COMMENT COERRZ=(TRNCOZ-THETAZ-GJKRPZ*WZEST)*ACSON
COMMENT XCONON=COMPAR(COERRX,ACSDB)-COMPAR(-ACSDB,COERRX)
COMMENT YCONON=COMPAR(COERRY,ACSDB)-COMPAR(-ACSDB,COERRY)
COMMENT ZCONON=COMPAR(COERRZ,ACSDB)-COMPAR(-ACSDB,COERRZ)

COMMENT ACS GAS JET FIRING LOGIC

COMMENT IF (GJON.LT.0.5) GO TO NOGJ

 NOGJ.. CONTINUE

COMMENT ******** REACTION WHEEL RATE+POSITION ATTITUDE CONTROL ********

        TDESRX=-RWKPTX*((THETAX-TRNCOX)+RWKRPX*WXEST)*ACSON
        TDESRY=-RWKPTY*((THETAY-TRNCOY)+RWKRPY*WYEST)*ACSON
        TDESRZ=-RWKPTZ*((THETAZ-TRNCOZ)+RWKRPZ*WZEST)*ACSON
```

```
COMMENT  ********************** TCS ALGORITHMS ************************

         INTERX=INTERX+SCXEST*ACSINC
         INTERY=INTERY+SCYEST*ACSINC
         INTERZ=INTERZ+SCZEST*ACSINC

         DFERRX=(-SCXEST-INTERX*DFINKX-DFKRPX*SCXDES)*TCSON
         DFERRY=(-SCYEST-INTERY*DFINKY-DFKRPY*SCYDES)*TCSON
         DFERRZ=(-SCZEST-INTERZ*DFINKZ-DFKRPZ*SCZDES)*TCSON

         DFXCON=COMPAR(DFERRX,TCSDB)-COMPAR(-TCSDB,DFERRX)
         DFYCON=COMPAR(DFERRY,TCSDB)-COMPAR(-TCSDB,DFERRY)
         DFZCON=COMPAR(DFERRZ,TCSDB)-COMPAR(-TCSDB,DFERRZ)

         IF (SCZDES.GT.-0.0005.AND.SCZEST.LT.ZDBOFF) DFZCON=1.0

COMMENT  TCS GAS JET FIRING LOGIC

         IF (DFON.LT.0.5) GO TO NODF

         IF (DFXCON) XN,XOFF,XP
   XN..  JETON(11)=1.0 $ JETON(16)=1.0 $ JETON(3)=1.0 $ JETON(7)=1.0
         GO TO XOFF
   XP..  JETON(12)=1.0 $ JETON(15)=1.0 $ JETON(3)=1.0 $ JETON(7)=1.0
 XOFF..  CONTINUE

         IF (DFYCON) YN,YOFF,YP
   YN..  JETON(10)=1.0 $ JETON(13)=1.0 $ JETON(1)=1.0 $ JETON(5)=1.0
         GO TO YOFF
   YP..  JETON(9) =1.0 $ JETON(14)=1.0 $ JETON(1)=1.0 $ JETON(5)=1.0
 YOFF..  CONTINUE

         IF (DFZCON) ZN,ZOFF,ZP
   ZN..  JETON(11)=1.0 $ JETON(12)=1.0 $ JETON(15)=1.0 $ JETON(16)=1.0
         GO TO ZOFF
   ZP..  JETON(2) =1.0 $ JETON(4) =1.0 $ JETON(6) =1.0 $ JETON(8) =1.0
 ZOFF..  CONTINUE

 NODF..  CONTINUE


COMMENT  ********************** GAS JET FUEL USAGE ************************

         NJETON=0.0
         DO SUMJ J=1,16
         NJETON=NJETON+JETON(J)
 SUMJ..  CONTINUE
         GASUSE=GASUSE+NJETON*GMFLOW*GJMOT

COMMENT  ************************************************************
COMMENT  ************** ESTIMATOR PERFORMANCE EVALUATION **************
COMMENT  ************************************************************

         ABERZ=ABS(SCZEST-SCZPM)          $       ERZ=ERZ+ABERZ
         ABERZD=ABS(SCZDES-SCZDPM)        $       ERZD=ERZD+ABERZD
```

```
COMMENT ************************************************************
COMMENT ***************** FORCES AND TORQUES ON S/C ******************
COMMENT ************************************************************

        FSCX=FGJX+FDISTX                          $      FSC(1)=FSCX
        FSCY=FGJY+FDISTY                          $      FSC(2)=FSCY
        FSCZ=FGJZ+FDISTZ                          $      FSC(3)=FSCZ
        TSCX=TGJX+TRWX+TDISTX                     $      TSC(1)=TSCX
        TSCY=TGJY+TRWY+TDISTY                     $      TSC(2)=TSCY
        TSCZ=TGJZ+TRWZ+TDISTZ                     $      TSC(3)=TSCZ

COMMENT ******************** ESTIMATOR FORCE MODEL ***********************

        ESTFMX=FGJX+FSR*SIN(THETAY-NADIRY)
        ESTFMY=FGJY
        ESTFMZ=FGJZ-FSR*COS(THETAY-NADIRY)

COMMENT ************************************************************

DERIVATIVE STAR     $     CINTERVAL  CI=0.010     $     HMINT=1.E-10
  XERROR WX =1.E-4 ,WY =1.E-4 ,WZ =1.E-4
  MERROR WX =1.E-4 ,WY =1.E-4 ,WZ =1.E-4
NOSORT
        NXQDER=NXQDER+1.

COMMENT ************************************************************
COMMENT ********************* PM AND S/C DYNAMICS ********************
COMMENT ************************************************************

COMMENT PM MOTION IN INERTIAL COORDINATES

        PMXDD=0.0     $    PMYDD=0.0     $    PMZDD=-SCZPM*IDK2*IDVOLT**2
        PMXD =0.0     $    PMYD =0.0     $    PMZD =INTEG(PMZDD,PMZDI)
        PMX  =0.0     $    PMY  =0.0     $    PMZ  =INTEG(PMZD,PMZI)

COMMENT ********** S/C ACCELERATIONS IN INERTIAL COORDINATES **********

        WXD,WYD,WZD=HCK(RATE,SCINRT,WX,WY,WZ,TSCX,TSCY,TSCZ)
        SCXDD=FSCX/SCMASS  $  SCYDD=FSCY/SCMASS  $  SCZDD=FSCZ/SCMASS

COMMENT ******************** S/C RATES AND POSITIONS *******************

        WX      =INTEG(WXD,WXI)
        WY      =INTEG(WYD,WYI)
        WZ      =INTEG(WZD,WZI)
        PZD,P1D,P2D,P3D=HCK(HCK,PZ,P1,P2,P3,WX,WY,WZ)
        PZ      =INTEG(PZD,PZI)
        P1      =INTEG(P1D,P1I)
        P2      =INTEG(P2D,P2I)
        P3      =INTEG(P3D,P3I)
        SCXD    =INTEG(SCXDD,SCXDI)
        SCYD    =INTEG(SCYDD,SCYDI)
        SCZD    =INTEG(SCZDD,SCZDI)
        SCX     =INTEG(SCXD,SCXI)
        SCY     =INTEG(SCYD,SCYI)
        SCZ     =INTEG(SCZD,SCZI)
```

```
COMMENT  ************************************************************
COMMENT  ********************* DISTURBANCE MODEL ********************
COMMENT  ************************************************************

         IF (DISTON.LT.0.5) GO TO NODIST

         RANDOM=OU(FSRCTC,T,FSRSIG,FSR)
         FDISTX=RANDOM*SIN(THETAY-NADIRY)
         FDISTY=0.0
         FDISTZ=-RANDOM*COS(THETAY-NADIRY)

 COMMENT CENTER OF PRESSURE CALCULATION
 COMMENT CPX=0.0          $          CPY=0.0          $          CPZ=0.0
 COMMENT CMTCPX=CPX-SCCMLV(1)
 COMMENT CMTCPY=CPY-SCCMLV(2)
 COMMENT CMTCPZ=CPZ-SCCMLV(3)

 COMMENT TDISTX=+FDISTZ*CMTCPY-FDISTY*CMTCPZ
 COMMENT TDISTY=-FDISTZ*CMTCPX+FDISTX*CMTCPZ
 COMMENT TDISTZ=+FDISTY*CMTCPX-FDISTX*CMTCPY

NODIST.. CONTINUE

 COMMENT ************************************************************
 COMMENT ************** REACTION WHEEL INDUCED DYNAMICS ***************
 COMMENT ************************************************************

         TRWX=(BOUND(-TRWMAX,+TRWMAX,TDESRX))*RWON
         TRWY=(BOUND(-TRWMAX,+TRWMAX,TDESRY))*RWON
         TRWZ=(BOUND(-TRWMAX,+TRWMAX,TDESRZ))*RWON

 COMMENT ************************************************************
 COMMENT ********** GAS JET INDUCED DYNAMICS ***********************
 COMMENT ************************************************************

         K=0      $      FGJ(1)=0.0      $      FGJ(2)=0.0      $      FGJ(3)=0.0
         DO SUMF J=1,7,2
         K=K+1    $    JP1=J+1    $    JP8=J+8 $    JP9=J+9
         DO SUMF JJ=1,3
         FGJC(K,JJ)=GJFV(J,JJ)*JETON(J)+GJFV(JP1,JJ)*JETON(JP1)+          ...
                    GJFV(JP8,JJ)*JETON(JP8)+GJFV(JP9,JJ)*JETON(JP9)
         FGJ(JJ)=FGJ(JJ)+FGJC(K,JJ)
   SUMF.. CONTINUE
         FGJX=FGJ(1)        $        FGJY=FGJ(2)        $        FGJZ=FGJ(3)

         TGJX=0.0           $        TGJY=0.0           $        TGJZ=0.0
         DO SUMT J=1,4
         TGJC(J,1)=+FGJC(J,3)*CMTGJV(J,2)-FGJC(J,2)*CMTGJV(J,3)
         TGJC(J,2)=-FGJC(J,3)*CMTGJV(J,1)+FGJC(J,1)*CMTGJV(J,3)
         TGJC(J,3)=+FGJC(J,2)*CMTGJV(J,1)-FGJC(J,1)*CMTGJV(J,2)
         TGJX=TGJX+TGJC(J,1)
         TGJY=TGJY+TGJC(J,2)
         TGJZ=TGJZ+TGJC(J,3)
   SUMT.. CONTINUE
```

```
COMMENT ******* S/C ACCELERATION, RATE, POSITION RELATIVE TO PM *******

        SCXAPM=SCXDD-PMXDD  $   SCYAPM=SCYDD-PMYDD  $   SCZAPM=SCZDD-PMZDD
        SCXDPM=SCXD-PMXD    $   SCYDPM=SCYD-PMYD    $   SCZDPM=SCZD-PMYD
        SCXPM=SCX-PMX       $   SCYPM=SCY-PMY       $   SCZPM=SCZ-PMY

COMMENT ************************************************************
COMMENT ****************** TCS ESTIMATOR EQUATIONS ******************
COMMENT ************************************************************

        CMAX=ESTFMX/SCMASS+PMXDD
        CMAY=ESTFMY/SCMASS+PMYDD
        CMAZ=ESTFMZ/SCMASS+PMZDD

        FP21  =P11*(WY*WY+WZ*WZ)+P31*(WZD-WX*WY)+2.0*P41*WZ-P51      ...
          *(WYD+WX*WZ)-2.0*P61*WY
        FP22  =P21*(WY*WY+WZ*WZ)+P32*(WZD-WX*WY)+2.0*P42*WZ-P52      ...
          *(WYD+WX*WZ)-2.0*P62*WY
        FP23  =P31*(WY*WY+WZ*WZ)+P33*(WZD-WX*WY)+2.0*P43*WZ-P53      ...
          *(WYD+WX*WZ)-2.0*P63*WY
        FP24  =P41*(WY*WY+WZ*WZ)+P43*(WZD-WX*WY)+2.0*P44*WZ-P54      ...
          *(WYD+WX*WZ)-2.0*P64*WY
        FP25  =P51*(WY*WY+WZ*WZ)+P53*(WZD-WX*WY)+2.0*P54*WZ-P55      ...
          *(WYD+WX*WZ)-2.0*P65*WY
        FP26  =P61*(WY*WY+WZ*WZ)+P63*(WZD-WX*WY)+2.0*P64*WZ-P65      ...
          *(WYD+WX*WZ)-2.0*P66*WY
        FP41  =-P11*(WZD+WX*WY)-2.0*P21*WZ+P31*(WX*WX+WZ*WZ)+P51     ...
          *(WXD-WY*WZ)+2.0*P61*WX
        FP42  =-P21*(WZD+WX*WY)-2.0*P22*WZ+P32*(WX*WX+WZ*WZ)+P52     ...
          *(WXD-WY*WZ)+2.0*P62*WX
        FP43  =-P31*(WZD+WX*WY)-2.0*P32*WZ+P33*(WX*WX+WZ*WZ)+P53     ...
          *(WXD-WY*WZ)+2.0*P63*WX
        FP44  =-P41*(WZD+WX*WY)-2.0*P42*WZ+P43*(WX*WX+WZ*WZ)+P54     ...
          *(WXD-WY*WZ)+2.0*P64*WX
        FP45  =-P51*(WZD+WX*WY)-2.0*P52*WZ+P53*(WX*WX+WZ*WZ)+P55     ...
          *(WXD-WY*WZ)+2.0*P65*WX
        FP46  =-P61*(WZD+WX*WY)-2.0*P62*WZ+P63*(WX*WX+WZ*WZ)+P65     ...
          *(WXD-WY*WZ)+2.0*P66*WX
        FP61  =P11*(WYD-WX*WZ)+2.0*P21*WY-P31*(WXD+WY*WZ)-2.0*       ...
          P41*WX+P51*(WX*WX+WY*WY)
        FP62  =P21*(WYD-WX*WZ)+2.0*P22*WY-P32*(WXD+WY*WZ)-2.0*       ...
          P42*WX+P52*(WX*WX+WY*WY)
        FP63  =P31*(WYD-WX*WZ)+2.0*P32*WY-P33*(WXD+WY*WZ)-2.0*       ...
          P43*WZ+P53*(WX*WX+WY*WY)
        FP64  =P41*(WYD-WX*WZ)+2.0*P42*WY-P43*(WXD+WY*WZ)-2.0*       ...
          P44*WZ+P54*(WX*WX+WY*WY)
        FP65  =P51*(WYD-WX*WZ)+2.0*P52*WY-P53*(WXD+WY*WZ)-2.0*       ...
          P54*WZ+P55*(WX*WX+WY*WY)
        FP66  =P61*(WYD-WX*WZ)+2.0*P62*WY-P63*(WXD+WY*WZ)-2.0*       ...
          P64*WZ+P65*(WX*WX+WY*WY)

        D11   =P11*P11+P31*P31+P51*P51
        D21   =P11*P21+P31*P32+P51*P52
        D31   =P11*P31+P31*P33+P51*P53
        D41   =P11*P41+P31*P43+P51*P54
        D51   =P11*P51+P31*P53+P51*P55
        D61   =P11*P61+P31*P63+P51*P65
```

```
D22    =P21*P21+P32*P32+PS2*PS2
D32    =P21*P31+P32*P33+PS2*PS3
D42    =P21*P41+P32*P43+PS2*PS4
DS2    =P21*PS1+P32*PS3+PS2*PS5
D62    =P21*P61+P32*P63+PS2*P65
D33    =P31*P31+P33*P33+PS3*PS3
D43    =P31*P41+P33*P43+PS3*PS4
DS3    =P31*PS1+P33*PS3+PS3*PS5
D63    =P31*P61+P33*P63+PS3*P65
D44    =P41*P41+P43*P43+PS4*PS4
DS4    =P41*PS1+P43*PS3+PS4*PS5
D64    =P41*P61+P43*P63+PS4*P65
DS5    =PS1*PS1+PS3*PS3+PS5*PS5
D65    =PS1*P61+PS3*P63+PS5*P65
D66    =P61*P61+P63*P63+P65*P65

P11    =INTEG(2.0*P21-R*D11,P11I)
P21    =INTEG(P22+FP21-R*D21,0.0)
P31    =INTEG(P32+P41-R*D31,0.0)
P41    =INTEG(P42+FP41-R*D41,0.0)
PS1    =INTEG(PS2+P61-R*   DS1,0.0)
P61    =INTEG(P62   +FP61-R*D61,0.0)
P22    =INTEG(2.0*FP22+SGPX-R*D22,P22I)
P32    =INTEG(P42+FP23-R*D32,0.0)
P42    =INTEG(FP42+FP24-R*D42,0.0)
PS2    =INTEG(P62+FP25-R*DS2,0.0)
P62    =INTEG(FP62+FP26-R*D62,0.0)
P33    =INTEG(2.0*P43-R*D33,P33I)
P43    =INTEG(FP43+P44-R*D43,0.0)
PS3    =INTEG(P63*     PS4-R*DS3,0.0)
P63    =INTEG(FP63+P64-R*D63,0.0)
P44    =INTEG(2.0*FP44+SGPY-R*D44,P44I)
PS4    =INTEG(P64+FP45-R*DS4,0.0)
P64    =INTEG(FP64+FP46-R*D64,0.0)
PS5    =INTEG(2.0*P65-R*DS5,PS5I)
P65    =INTEG(FP65+P66-R*D65,0.0)
P66    =INTEG(2.0*FP66+SGPZ-R*D66,P66I)

LLXH   =SCXEST-SCCMXE       $     LLXHD=SCXDES
LLYH   =SCYEST-SCCMYE       $     LLYHD=SCYDES
LLZH   =SCZEST-SCCMZE       $     LLZHD=SCZDES

XHDD   =+CMAX+(WY*WY+WZ*WZ)*LLXH+(WZD-WX*WY)*LLYH                    ...
         +2.0*WZ*LLYHD-(WYD-WX*WZ)*LLZH-2.0*WY*LLZHD
YHDD   =+CMAY-(WZD+WX*WY)*LLXH-2.0*WZ*LLXHD+(WX*WX                   ...
         +WZ*WZ)*LLYH+(WXD-WY*WZ)*LLZH+2.0*WX*LLZHD
ZHDD   =+CMAZ+(WYD-WX*WZ)*LLXH+2.0*WY*LLXHD-(WXD                     ...
         +WY*WZ)*LLYH   -2.0*WX*LLYHD+(WX*WX+WY*WY)*LLZH
```

```
COMMENT ESTIMATED S/C RATES AND POSITIONS RELATIVE TO THE PM

          SCXEST=INTEG(SCXDES+R*(P11*(SCXOB-SCXEST)+P31*(SCYOB-SCYEST)...
                 +P51*(SCZOB-SCZEST)),SCXESI)
          SCXDES=INTEG(XHDD+R*(P21*(SCXOB-SCXEST)+P32*(SCYOB-SCYEST)  ...
                 +P52*(SCZOB-SCZEST)),SCXDEI)
          SCYEST=INTEG(SCYDES+R*(P21*(SCXOB-SCXEST)+P33*(SCYOB-SCYEST)...
                 +P53*(SCZOB-SCZEST)),SCYESI)
          SCYDES=INTEG(YHDD+R*(P41*(SCXOB-SCXEST)+P43*(SCYOB-SCYEST)  ...
                 +P54*(SCZOB-SCZEST)),SCYDEI)
          SCZEST=INTEG(SCZDES+R*(P51*(SCXOB-SCXEST)+P53*(SCYOB-SCYEST)...
                 +P55*(SCZOB-SCZEST)),SCZESI)
          SCZDES=INTEG(ZHDD+R*(P61*(SCXOB-SCXEST)+P63*(SCYOB-SCYEST)  ...
                 +P65*(SCZOB-SCZEST)),SCZDEI)

 COMMENT ************************************************************
 COMMENT ************************************************************
 COMMENT ************************************************************

END
END
END
TERMINAL
   FIN.. CONTINUE
   AVERX=ERX/NXQDYN     $     AVERXD=ERXD/NXQDYN
   AVERY=ERY/NXQDYN     $     AVERYD=ERYD/NXQDYN
   AVERZ=ERZ/NXQDYN     $     AVERZD=ERZD/NXQDYN
   DEBUG
   NXQTER=NXQTER+1.
   WRITE(6,F2)T,NXQINT,NXQDYN,NXQDER,NXQTER,DERPDY
   F2.. FORMAT (1X,6G14.8)

END
END
```

APPENDIX D

CHARGE ESTIMATION SIMULATIONS AND COMPUTER PROGRAM

Fig. 4.1. The terminal values of this estimator are within 3% - 4% of the true value. But note how much the estimate varies in the first 300 seconds.

Simulation #1

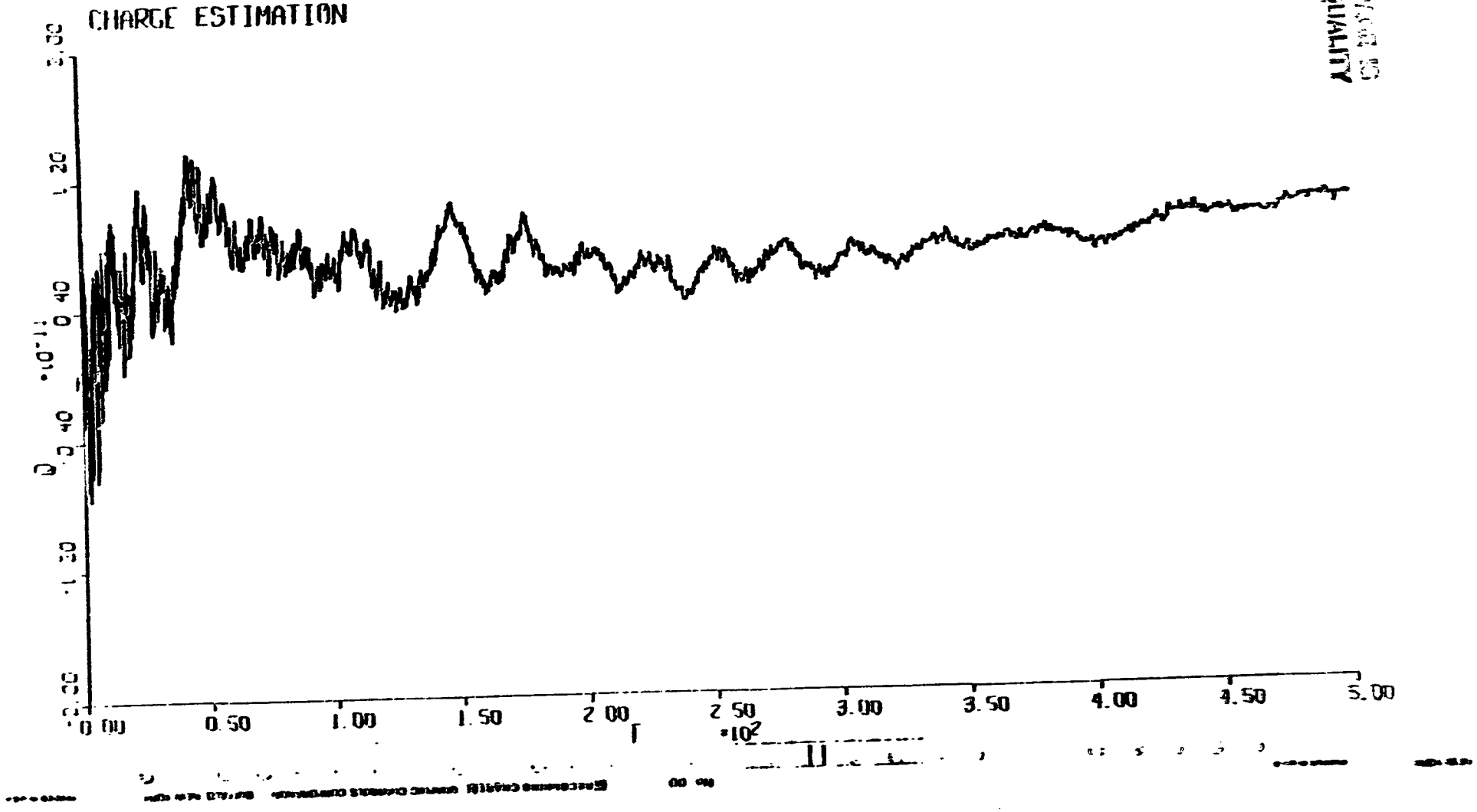

Fig. 4.2. This simulation illustrates how disruptive unmodeled disturbances can become. Here the correlation time of the disturbance coincides with the period of the plate excitation. Note that the estimate ultimately appears to be converging, but to the wrong value.

Simulation #2

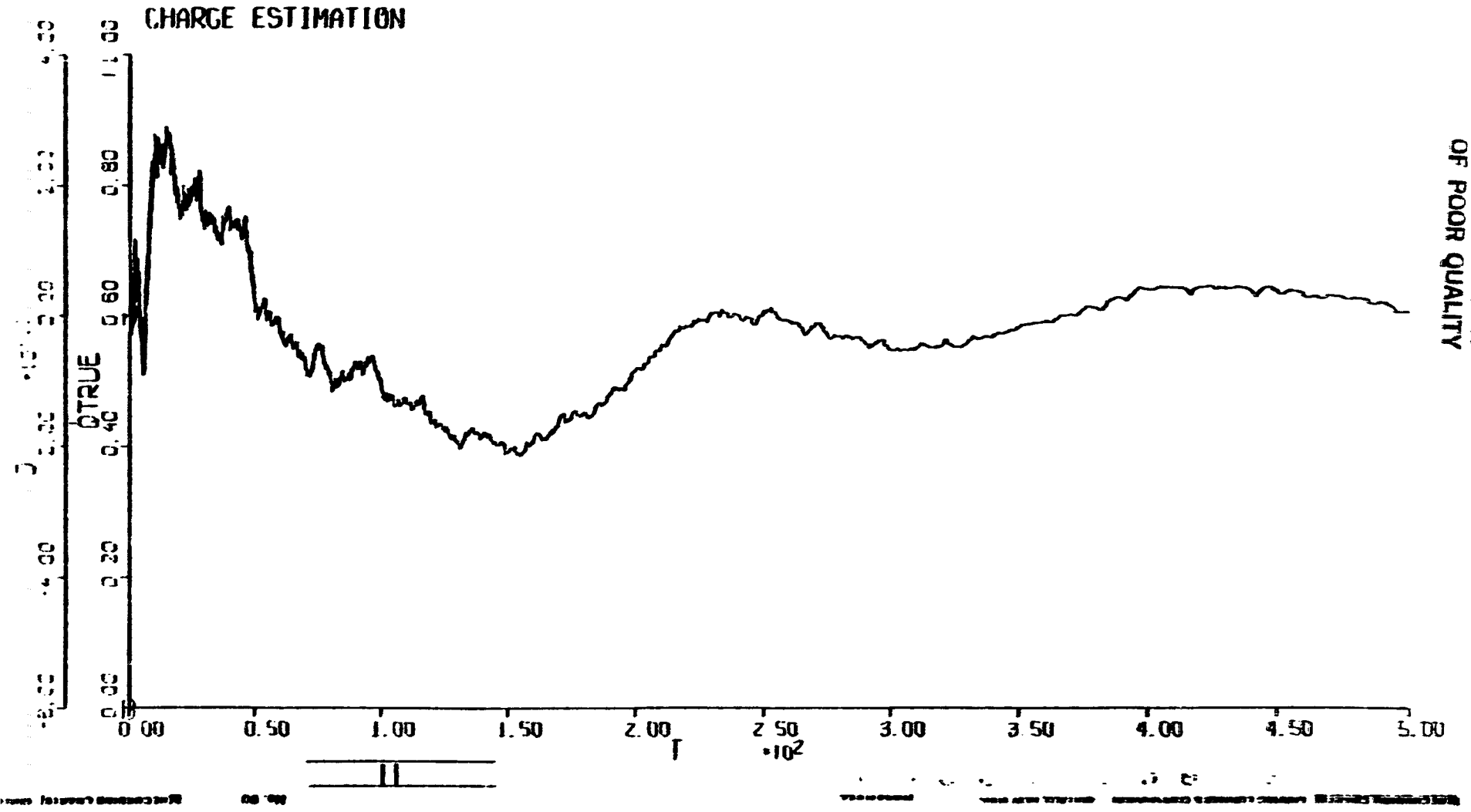

Fig. 4.3. This simulation illustrates the impact of lower voltage on estimator performance. Note how much smoother the other estimators are in comparison. This can be attributed to the fact that the gains of this estimator are decreasing more slowly.

Simulation #9

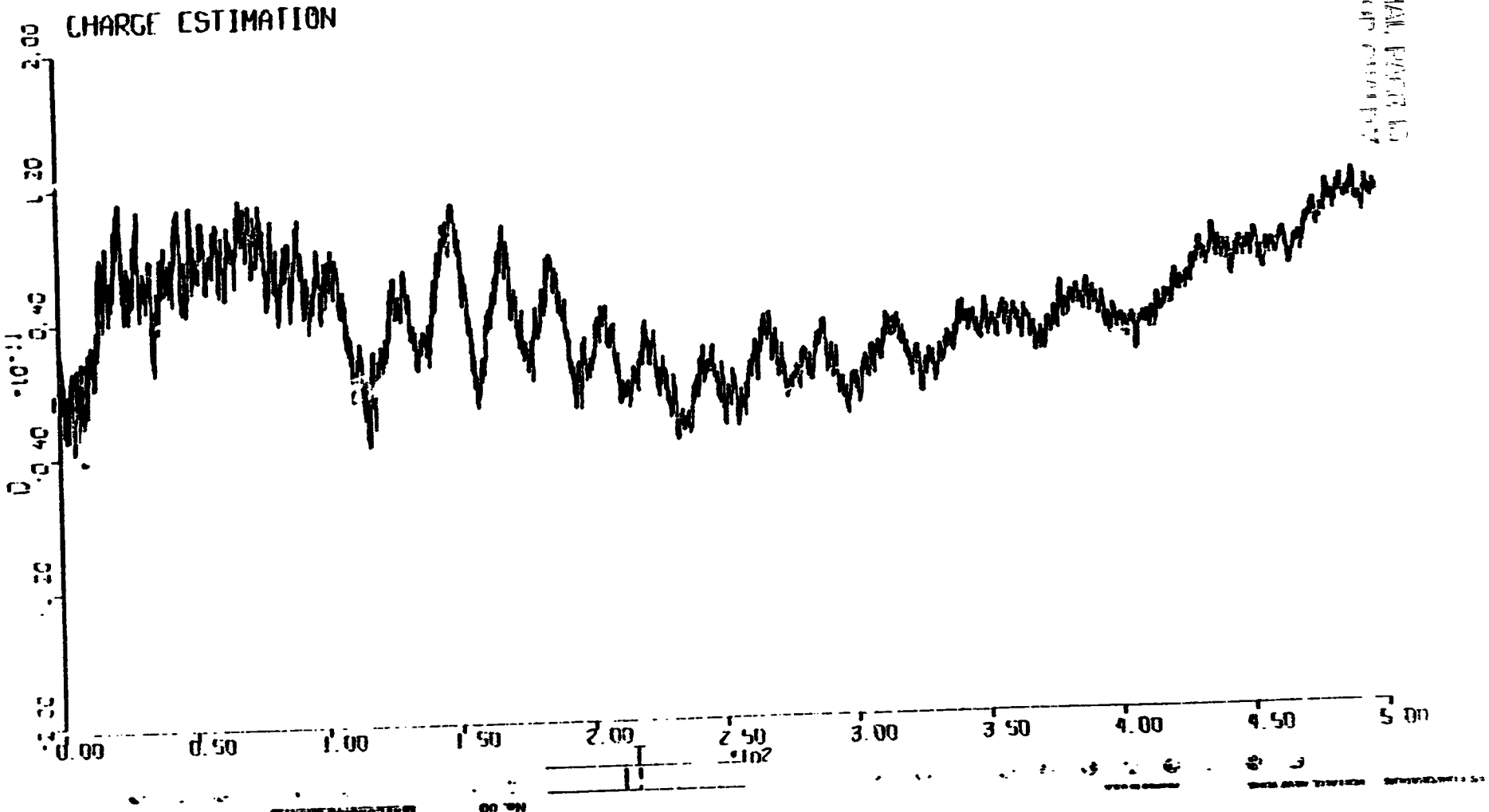

g. 4.4. This plot dramatizes the accuracy requirement
increasing charge. The barely perceptible squiggles
the estimate are enough to make this estimator
reliable.

aulation #13

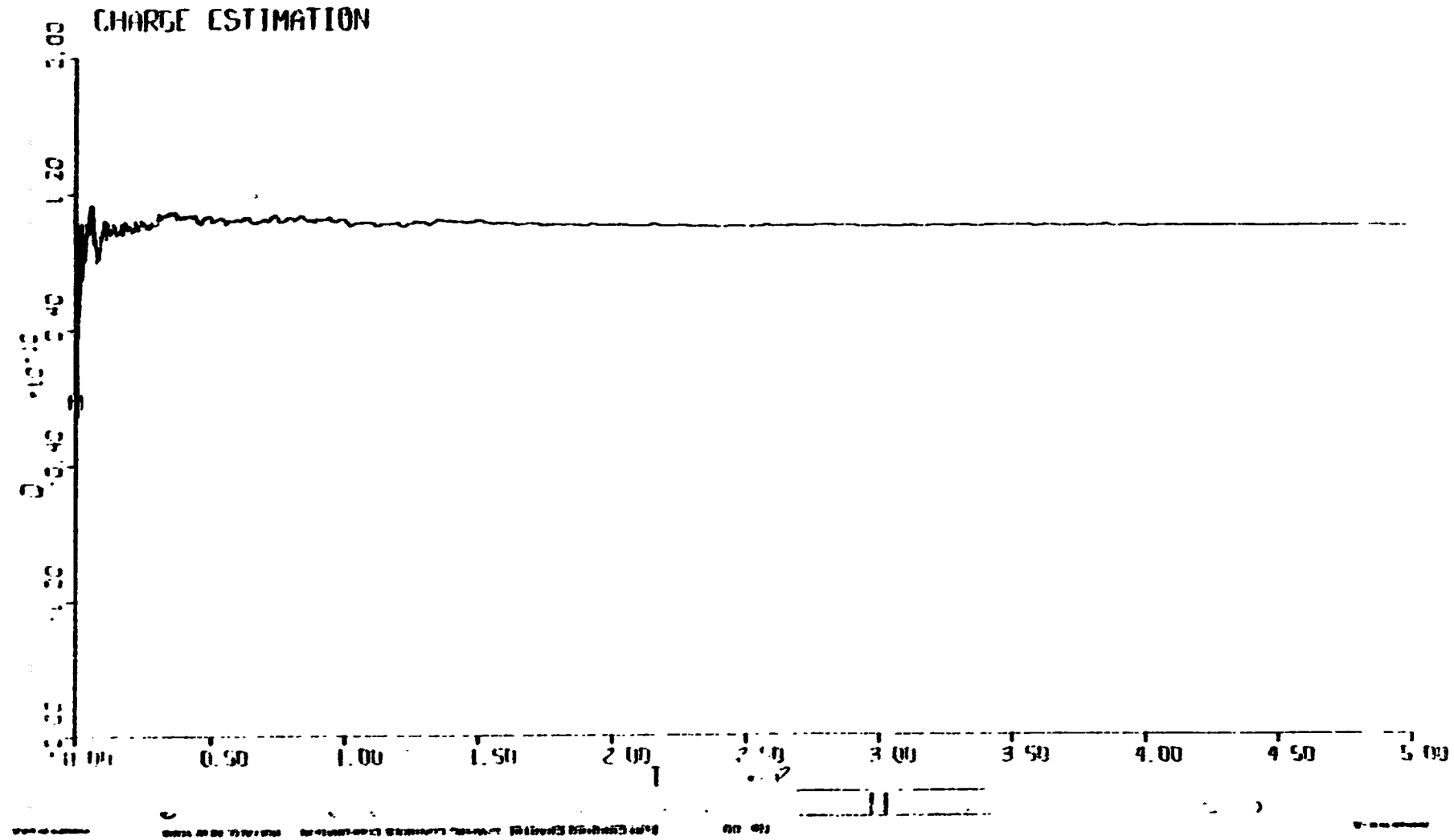

PENDIX D

arge Estimation Program

```
IN DRAG3, H1BU8/MARK,57395,30/0
LK,F 125/180,LSPA
ELETE,C TFILE.
ELETE,C PRT.
ELETE,C PLT.
SG,T TFILE.
SG,UP PLT.
*KPT PUNCHS/PLT
SG,A ACSL*ACSL.
SE MACDUM.,ACSL*ACSL.
SG,T 7.
CSL*ACSL.ABS TFILE,IS
OGRAM DRAGF
ITIAL
    CONSTANT      TSTOP=499.99
    *CAPACITANCE CONSTANTS*
    A         =3.317
    L         =6.424
    B         =.02
    HN        =1.466
    HR        =15.359
    E         =8.854E-12
    U         =1.0E7
    J1        =250
    EE        =8.854E-2
    P         =-1.203
    *CONTROL PARAMETERS AND INITIAL CONDITIONS*
    DB        =5.0E3
    BB        =.5
    K         =0.0
    KK1       =0.0
    F0        =0.0
    XX10      =-4.9E3
    XX20      =0.0
    *FILTER PARAMETERS*
    X10       =-4.9E3
    X20       =0.0
    Q0        =0.0
    V         =250.0
    Q0        =1.6E-11
    SGOX      =5.0
    R         =4.0
    P1        =1.0
    P2        =1.0
    VX        =100.0
    R0        =1.0E-21
    N         =10.0
    N1        =250.0
DS*OF INITIAL*
NAMIC
    CINT      =.01
    *CONTROL LOOP*
    Z         =XX1+BB*XX2
    E0        =ABS(Z)
    K         =K+1.0
    S         =RSW(Z.GE. 0.0, -1.0, 1.0)
    Y         =RSW(E0. GE. DB, 1.0, 0.0)
    IF(Y.GT.0.1) GO TO R0
    IF(K.LE.1.1) GO TO F
```

```
      P2        =1.0
      VX        =100.0
      RQ        =1.0E-21
      N         =10.0
      N1        =250.0
NDS*OF INITIAL*
YNAMIC
      CINT      =.01
      *CONTROL LOOP*
      Z         =XX1+BB*YX2
      EO        =ABS(Z)
      K         =K+1.0
      S         =RSW(Z.GE. 0.0, -1.0, 1.0)
      Y         =RSW(EO. GE. DB, 1.0, 0.0)
      IF(Y.GT.0.1) GO TO BO
      IF(K.LE.1.1) GO TO F
      Y         =1.0
      IF(K.LE.100.1) GO TO C
..    CONTINUE
      K         =0.0
      GO TO C
0..   CONTINUE
      K         =1.0
..    CONTINUE
      KK1       =KK1+1.0
      V1        =-V
      IF(KK1.GT.N1) GO TO F1
      GO TO F2
1..   V         =V1
      KK1       =0.0
2..   CONTINUE
      CN        =1.0E2+2.6E3*S*Y
      *GENERATION OF THE OBSERVATIONS*
      NOX       =GAUSS(0.0,SGOX)
      VX        =XX1+NOX
0..   CONTINUE
ERIVATIVE
      *GENERATION OF THE STATE*
      NX        =DU(25.0,0.0,50.0)
      XX1       =INTEG(XX2,XX10)
      XX2       =INTEG(U*V*QQ*P*(1.0/(B*HR))*A*E*J1*(2.0*L*...
      (V**2)-4.0*((P*A*V)**2)*1.0/HR)*XX1*QQ*...
      2.5E12*QQ*HN*(1.0/(EE*B*B*HR))*XX1*CN*NX,XX20)
      *FILTER EQUATIONS*
      F21       =E*J1*(2.0*L*(V**2)-4.0*((P*A*V...
      )**2)*1.0/HR)*Q*2.5E12*Q*HN*(1.0/(EE*B*B*HR))
      F23       =U*V*P*(1.0/(B*HR))*A*5.0E12*Q*HN*(1.0/(EE*...
      B*B*HR))*X1
      P11       =INTEG(2.0*P21-R*P11*P11,P1)
      P21       =INTEG(F21*P11+P22-R*P11*P21,0.0)
      P31       =INTEG(P32-R*P31*P11,0.0)
      P22       =INTEG(2.0*(F21*P21+F23*P32)+VX-R*P21*P21,P2)
      P32       =INTEG(F21*P31+F23*P33-R*P21*P31,0.0)
      P33       =INTEG(VQ-R*P31*P31,RQ)
      X1        =INTEG(X2+R*P11*(YX-X1),X10)
      X2        =INTEG(U*V*Q*P*(1.0/(B*HR))*A*F21*X1*CN*...
      R*P21*(YX-X1),X20)
      Q         =INTEG(R*P31*(YX-X1),QQ)
```

```
      P31       =INTEG(P32-R*P31*P11,0.0)
      P22       =INTEG(2.0*(F21*P21+F23*P32)*VX-R*P21*P21,P2)
      P32       =INTEG(F21*P31+F23*P33-R*P21*P31,0.0)
      P33       =INTEG(VQ-R*P31*P31,RQ)
      X1        =INTEG(X2*R*P11*(VX-X1),X10)
      X2        =INTEG(U*V*Q*P*(1.0/(B*HR))*A*F21*X1*CN*...
     R*P21*(VX-X1),X20)
      Q         =INTEG(R*P31*(VX-X1),Q0)
      GAIN      =R*P31
$DS*OF DERIVATIVE*
      TERMT(T.GE.TSTOP)
$DS*OF DYNAMIC*
$DS*OF PROGRAM*
FREE MACDUM.
ADD,ELP 7.
EOF
MAP,ISX MAP,TFILE.ABS
$ TPFS.
$ TFILE.
$ ACSL*ACSL.ZZDRAW/CAPPLT
$ BLANKSCOMMON
LIB ACSL*ACSL.
LIB LIB*PLOTS.
LIB LIB*JPLS.
LIB LIB*CLIBS.
$D
MDG,N .P,66,0,0
$GT  TFILE.ABS
ET TITLE='CHARGE ESTIMATION'
ET PSFCPL     =1.2
ET XINCPL     =10.0
ET DIS=99$'FORCE 3 COL FORMAT FOR OUTPUT'
ET CALPLT= .TRUE.
ET PRNPLT=.FALSE.
      OUTPUT T,Q,GAIN,P33,'NCICUT'=50
REPAR T,Q
START
PLOT Q
TOP
FREE PLT.
LNK,SUC PLT.,125/180,PLTA
FIN
```

CHARGING OF THE PROOF MASS DURING THE STARPROBE MISSION

This appendix is a summary of results given in a detailed study by M. Harel et al of JPL [7].

A preliminary analysis of charging of the proof mass during the Starprobe Mission reveals that the Jovian environment is the largest contributor of charging currents. For our study we performed quantitative estimates for the following environments: a) cosmic ray, b) Jovian environment (considering perijoves of 3Rj and 9Rj), c) Solar environment including the radiation due to solar flares.

We find that the cosmic rays will result in a positive charge of 3.3×10^{-11} coulomb for a five year mission. The Jovian environment will give a negative charge of $5.2\text{-}5.3 \times 10^{-7}$ coulomb. The typical large solar flare environment is expected to result in a maximum positive charge of about 1×10^{-10} coulomb which is also small compared to Jovian environment (see Table 1 below).

We should comment that this study will only give order-of-magnitude type results. To achieve better estimates of the charging currents one would have to do a more careful study that includes secondary particles, neutron fluxes and more precise trajectory. The table below summarizes our findings.

Table 1. Proof Mass Charging for Starprobe Mission

Phase	Electron Current (A/Cm^2)	Proton Current (A/Cm^2)	Net Current (A/Cm^2)	Charge Per Day (Coulomb/Cm^2-day)	Charge per Mission Phase Coulomb
Cosmic Ray	5.12×10^{-21}	6.09×10^{-20}	5.57×10^{-20}	4.8×10^{-15}	3.3×10^{-11}
Jupiter (3Rj)	4.67×10^{-12}	1.07×10^{-14}	-4.66×10^{-12}	-4.02×10^{-7}	-1.53×10^{-6} (1 day)
Jupiter (4Rj)	1.6×10^{-12}	1×10^{-16}	-1.6×10^{-12}	-1.38×10^{-7}	-5.2×10^{-7} (1 day)
Solar Enc.					
Typical Large Flare					1×10^{-10} (1 day)
Upper Limit					